Defense Threat Reduction Agency
8725 John J. Kingman Road, MS
6201 Fort Belvoir, VA 22060-6201

DTRA-TR-09-33

TECHNICAL REPORT

Interaction of Chemical Agents with Nanoscale Molecular Junctions

Approved for public release; distribution is unlimited.

August 2011

HDTRA01-07-C-0086

Prepared by:
SAIC
3465 Box Hill Corporate
Center Drive
Suite A
Abingdon, MD 21009

REPORT DOCUMENTATION PAGE

Form Approved
OMB No. 0704-0188

1. REPORT DATE *(DD-MM-YYYY)*	2. REPORT TYPE	3. DATES COVERED *(From - To)*
00-08-2011	Technical	

4. TITLE AND SUBTITLE
Interaction of Chemical Agents with Nanoscale Molecular Junctions

5a. CONTRACT NUMBER

5b. GRANT NUMBER

5c. PROGRAM ELEMENT NUMBER

6. AUTHOR(S)

5d. PROJECT NUMBER

5e. TASK NUMBER

5f. WORK UNIT NUMBER

7. PERFORMING ORGANIZATION NAME(S) AND ADDRESS(ES)

SAIC
3465 Box Hill Corporate Center
Suite A
Abingdon, MD 21009

8. PERFORMING ORGANIZATION REPORT NUMBER

9. SPONSORING / MONITORING AGENCY NAME(S) AND ADDRESS(ES)
Defense Threat Reduction Agency
8725 John J. Kingman Road, MS 6201
Fort Belvoir, VA 22060-6201
Stephen Lee/ US Army

10. SPONSOR/MONITOR'S ACRONYM(S)

11. SPONSOR/MONITOR'S REPORT NUMBER(S)
DTRA-TR-09-33

12. DISTRIBUTION / AVAILABILITY STATEMENT
Approved for public release; distribution is unlimited.

13. SUPPLEMENTARY NOTES

14. ABSTRACT
This report describes research from an SAIC contract with the Defense Threat Reduction Agency to support efforts under the Chemical and Biological Defense Initiative Fund (CBDIF). This research program examined the interaction of various chemical agents with molecular junctions and the electronic effects observed on charge transport through nanoscale meta-molecule-metal-devices. We utilized a magnetic self-assembly technique to fabricate in parallel molecular junctions which incorporated a variety of organic self-assembled monolayers (SAMs).

15. SUBJECT TERMS
Nanotechnology Molecular
SAMs Hydrocarbon

16. SECURITY CLASSIFICATION OF:			17. LIMITATION OF ABSTRACT	18. NUMBER OF PAGES	19a. NAME OF RESPONSIBLE PERSON
a. REPORT	b. ABSTRACT	c. THIS PAGE			19b. TELEPHONE NUMBER *(include area code)*
Unclassified	Unclassified	Unclassified	SAR	42	

CONVERSION TABLE

Conversion Factors for U.S. Customary to metric (SI) units of measurement.

MULTIPLY →	BY →	TO GET
TO GET ←	BY ←	DIVIDE

angstrom	1.000 000 x E -10	meters (m)
atmosphere (normal)	1.013 25 x E +2	kilo pascal (kPa)
bar	1.000 000 x E +2	kilo pascal (kPa)
barn	1.000 000 x E -28	meter^2 (m^2)
British thermal unit (thermochemical)	1.054 350 x E +3	joule (J)
calorie (thermochemical)	4.184 000	joule (J)
cal (thermochemical/cm^2)	4.184 000 x E -2	mega joule/m^2 (MJ/m^2)
curie	3.700 000 x E +1	*giga bacquerel (GBq)
degree (angle)	1.745 329 x E -2	radian (rad)
degree Fahrenheit	$t_k = (t°f + 459.67)/1.8$	degree kelvin (K)
electron volt	1.602 19 x E -19	joule (J)
erg	1.000 000 x E -7	joule (J)
erg/second	1.000 000 x E -7	watt (W)
foot	3.048 000 x E -1	meter (m)
foot-pound-force	1.355 818	joule (J)
gallon (U.S. liquid)	3.785 412 x E -3	meter^3 (m^3)
inch	2.540 000 x E -2	meter (m)
jerk	1.000 000 x E +9	joule (J)
joule/kilogram (J/kg) radiation dose absorbed	1.000 000	Gray (Gy)
kilotons	4.183	terajoules
kip (1000 lbf)	4.448 222 x E +3	newton (N)
kip/inch^2 (ksi)	6.894 757 x E +3	kilo pascal (kPa)
ktap	1.000 000 x E +2	newton-second/m^2 ($N-s/m^2$)
micron	1.000 000 x E -6	meter (m)
mil	2.540 000 x E -5	meter (m)
mile (international)	1.609 344 x E +3	meter (m)
ounce	2.834 952 x E -2	kilogram (kg)
pound-force (lbs avoirdupois)	4.448 222	newton (N)
pound-force inch	1.129 848 x E -1	newton-meter (N-m)
pound-force/inch	1.751 268 x E +2	newton/meter (N/m)
pound-force/foot^2	4.788 026 x E -2	kilo pascal (kPa)
pound-force/inch^2 (psi)	6.894 757	kilo pascal (kPa)
pound-mass (lbm avoirdupois)	4.535 924 x E -1	kilogram (kg)
pound-mass-foot^2 (moment of inertia)	4.214 011 x E -2	kilogram-meter^2 ($kg-m^2$)
pound-mass/foot^3	1.601 846 x E +1	kilogram-meter^3 (kg/m^3)
rad (radiation absorbed dose)	1.000 000 x E -2	**Gray (Gy)
roentgen	2.579 760 x E -4	coulomb/kilogram (C/kg)
shake	1.000 000 x E -8	second (s)
slug	1.459 390 x E +1	kilogram (kg)
torr (mm Hg, 0^0 C)	1.333 22 x E -1	kilo pascal (kPa)

*The Becquerel (Bq) is the SI unit of radioactivity; 1 Bq = 1 event/s.
**The Gray (Gy) is the SI unit of absorbed dose.

Abstract:

The following report describes research from an SAIC contract with the Defense Threat Reduction Agency to support efforts under the Chemical and Biological Defense Initiative Fund (CBDIF). This research program examined the interaction of various chemical agents with molecular junctions and the electronic effects observed on charge transport through nanoscale metal-molecule-metal devices. We utilized a magnetic self-assembly technique to fabricate in parallel molecular junctions which incorporated a variety of organic self-assembled monolayers (SAMs) functionalized with reactive chemical substituents chosen for their ability to bind vapor-phase compounds of interest. Changes in electron transport through incorporated SAMs were correlated to chemical interactions observed using reflectance FT-IR of the SAMs on gold. Real-time current-voltage (I-V) measurements, coupled with reflectance FT-IR have been combined to yield valuable information as to the interactions occurring between functionalized self-assembled monolayers immobilized in a molecular junction and gaseous chemical agents of interest to the defense community. The information contained in this report could yield valuable information for the possible development of nanoscale sensors using organic receptors and molecular charge transport.

Introduction:

There is currently strong interest to understand the physical and chemical interactions which take place when materials are exposed to toxic compounds of interest to the defense community. Although a variety of surface interactions are commonly studied using a number of analytical techniques (e.g. infrared spectroscopy), it has been difficult to examine interactions taking place between single or small assemblies of molecules on the nanoscale. Such techniques are desired due to the increasing use of nanotechnology in both the military and civilian sectors. Knowledge of the chemical interactions which occur on the surface of nanoparticles or within nanometer-thick self-assembled monolayers are essential for understanding the unique reactions chemical compounds can undergo when exposed to these novel materials. In addition, the characterization of reversible surface interactions, such as hydrogen-bonding or metal-ligand coordination, is a topic which is virtually unexplored on the nanoscale.

In the field of nanoscience known as molecular electronics,[1,2] it has become clear that the local chemical environment around molecules which support electron transport plays a dominant role in the conductivity of organic molecules. Morphology and structure of the monolayer, chemical functionality, and molecular environment have all been demonstrated to influence electrical conduction through organic molecules held within nanoscale junctions.[3-5] In addition to these variables, another important influence dictating molecular conductance is absorbent penetration into the structure of the monolayer or thin-film. Although studies examining chemical reactions on monolayer surfaces have been abundant in the literature,[6,7] few have focused on molecular adsorption into the monolayer bulk structure or the resulting effects induced on charge transport through individual or small aggregates of molecules.[8,9]

Recently, our group reported a new method for fabricating nanoscale molecular junctions based on the magnetic-directed assembly of electrically conductive microspheres onto SAM-functionalized source-drain electrodes.[10,11] This method of nanoelectronic device fabrication exploits localized magnetic fields generated within a ferromagnetic array to direct the assembly of susceptible species to the high-field regions between micron-scale contacts. When an individual colloid bridges the electrodes of a device, an electrical contact is formed which includes the self-assembled monolayer bound to the surface of the electrodes. Current through the device is forced to flow through the incorporated molecules trapped between the colloid and the electrodes. Magnetic entrapment can be considered a "soft" self-assembly technique incapable of causing chemical reactions in the monolayer during the fabrication process, a problem encountered with several previous techniques.[12,13] Due to the small contact area achieved through the use of micron-scale spherical colloid, this method provides a simple means to fabricate nanoscale devices (~ 60 nm^2 area) which incorporate approximately 100-300 individual molecules. This novel technique has allowed us to fabricate nanoscale molecular junctions incorporating molecules with specific chemical functionality and to analyze interactions within an organic monolayer during exposure to a wide variety of chemical agents.

Figures 1 and 2 illustrate the basic steps involved in forming a microsphere molecular junction. The fabrication of magnetic and electrically conductive silica colloid is accomplished

through a two-step evaporative metallization process.[14,15] After formation of a close-packed monolayer of 1.5 μm diameter silica colloid on wafers of silicon (Figure 1a), we deposit nickel (50 nm) then gold (10 nm) forming a metallic bilayer on the spheres. The underlying layer of nickel provides the magnetic handle needed to manipulate the resulting colloid from a solution, while the thin gold overcoat yields an oxide-free surface for connecting to and measuring charge transport across an organic monolayer. After metallization, the prepared microspheres are dispersed in ethanol using sonication (Figure 1b). Entrapment of these particles is performed using magnetic micron-scale electrodes composed of vapor-deposited nickel encased in a thin layer of gold (Figures 2a and 2b). The underlying nickel provides the ferromagnetic layer needed to generate a magnetic field between the source/drain electrodes, while the thin gold overcoat yields an oxide-free surface to promote strong gold-sulfur coupling (thiol-monolayer formation) on the electrode surface and permit low resistant charge transport to and from the organic monolayer. Each device incorporates a set of probe tips separated by 0.5 – 1.0 μm where the locally intense magnetic field directs the placement of colloid. Best results are obtained when each device is placed in an external magnetic field (225 Gauss) during the trapping process. Deposition is performed for 30 minutes using a solution of dispersed colloid in anhydrous ethanol. Efficiency for single-bead entrapment is found to be approximately 60% (Figure 2e), while 20-30% of junctions incorporate 2-3 beads and 10-20% remain empty. Once deposited, we find our colloid can only be removed again by sonication, suggesting the devices are structurally robust.

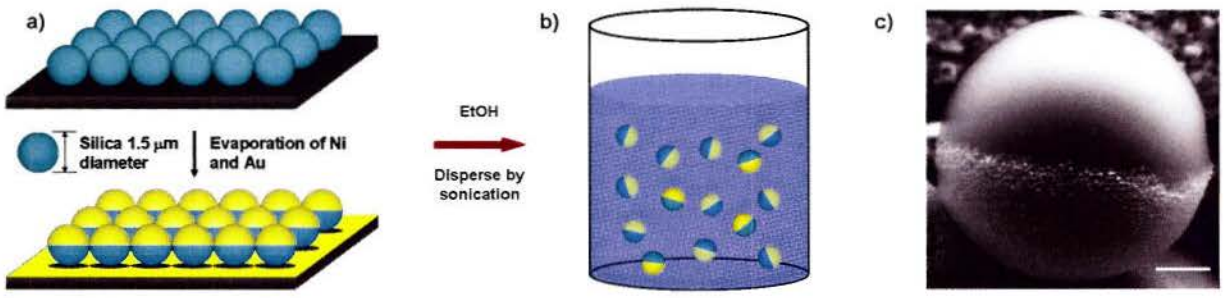

Figure 1. Fabrication of metallized silica colloid. **a)** A two-step metallization process produces electrically-conductive and magnetically-susceptible colloid suitable for device fabrication. **b)** Sonication in anhydrous ethanol produces a dispersed solution of the magnetic particles. **c)** SEM image showing the distinct hemisphere of deposited metal (10 nm gold over 50 nm nickel) on a colloid 1.5 μm in diameter. Scale bar = 300 nm.

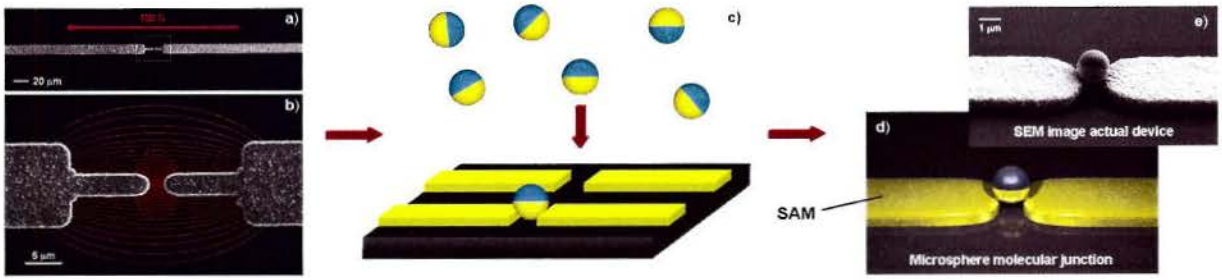

Figure 2. Magnetic assembly of microsphere molecular junctions. **a & b)** Scanning electron micrographs showing device structure, magnetic field lines shown schematically. **c)** Exposure of magnetized array to dispersed colloid in ethanol initiates assembly of the spheres at the location of intense magnetization. **d & e)** Images depicting final structure of a microsphere junction.

A major advantage of the microsphere test-bed is its ability to incorporate a wide variety of organic monolayers functionalized with chemical substituents capable of reaction with gaseous agents. The only requirement for use with this technique is that the molecules form a dense monolayer on the surface of the magnetic electrodes through the use of gold-sulfur coupling chemistry. The reaction of metal surfaces with organic ligands has become standard practice for many applications.[7,16] The high affinity thiol molecules display for the bare surface of several metals, in particular gold, render them extremely useful for the fabrication of self-assembled monolayers incorporating well-defined structure, orientation, and surface chemistry. In addition, the use of organic chemistry to produce a wide variety of functionalized thiol molecules has been demonstrated recently by several groups.[17,18] SAMs adopt highly regular two dimensional structures through spontaneous organization and provide a simple means to tailor the surface of many materials. Self-assembled monolayers are compatible with studies in nanotechnology since they offer easy deposition on surfaces of all sizes and morphologies from nanoparticles to porous surfaces, they can be used to mimic the chemical functionality of bulk materials in a thin surface film, and can be used to couple the external environment to the electronic properties of metal interconnect structures in order to monitor the current-voltage response in the SAM. Combined with the unique architecture of the microsphere test-bed, the properties of self-assembled monolayers are ideally suited for the study of how toxic chemicals in the vapor phase interact with various chemical functionalities found in organic monolayers.

Recently, our group has utilized the microsphere test-bed to perform a number of detailed studies of how chemical substituents on thiol molecules control the flow of electrons through molecular junctions.[10,11,19,20] It was during the course of this research that we first encountered the high sensitivity of nanoscale molecular junctions to their chemical environment. We found that the gaseous atmosphere a microsphere molecular junction is exposed to during electrical analysis can have a profound influence on the magnitude of current flowing through the devices.[20] Using non-functionalized alkanethiol and oligo(phenylene-ethynylene) (OPE) molecules to form dense self-assembled monolayers, we discovered that atmospheric water rapidly diffused into the molecular junctions and associated non-covalently to the sulfur headgroup of the molecules, hindering charge transport through each device. Our measurements revealed the diffusion of gases into our devices, followed by reaction with the incorporated SAM, was complete in 1-4 seconds, suggesting rapid diffusion into the nanoscale device and adsorption into the film. We subsequently discovered that similar penetration of gold-thiol SAMs by a wide variety of vapor-phase organics was also possible.

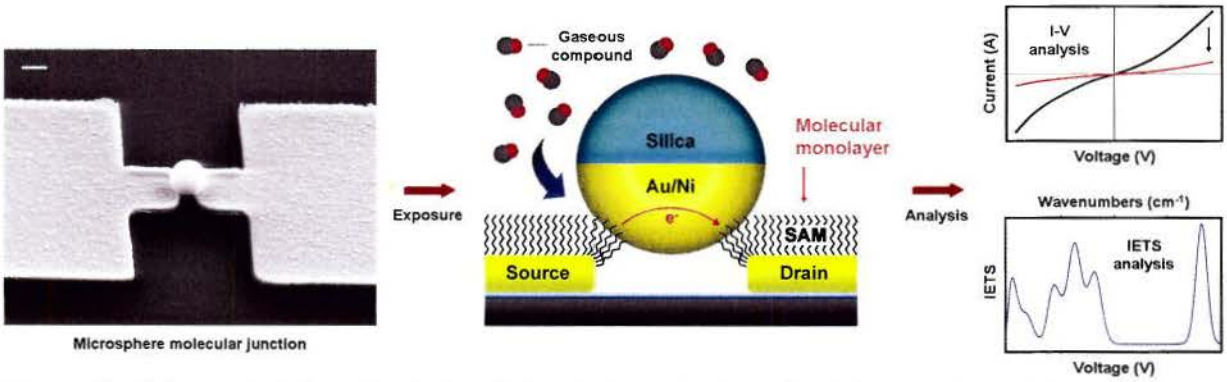

Figure 3. Scheme depicting the study of chemical agent adsorption into nanoscale molecular junctions. The "open" architecture of a microsphere molecular junction allows the rapid diffusion of gases into the nanoscale device and interaction with the molecules in the monolayer which support charge transport. Interactions can be monitored using current-voltage (I-V) measurements and inelastic electron tunneling spectroscopy (IETS).

The research project described in this report used similar techniques to study in detail the interaction of vapor-phase chemical agents with nanoscale molecular monolayers and devices. This research is based on the proposition that if non-functionalized SAMs show prominent interactions with ordinary atmospheric gases, then specially designed highly functionalized molecules could be used to study the interaction with vapor-phase toxic compounds of interest to

the defense community. Figure 3 shows the basic scheme depicting the use of microsphere molecular junctions to study the interaction of chemical agents with a functionalized monolayer. Because microsphere junctions incorporate an open architecture which allows the rapid diffusion of the surrounding atmosphere into each device, we studied during the course of this project how chemical agents adsorb and interact with chemically-functionalized monolayers held within the rigid environment of nanoscale molecular junction.

This report presents data gathered using microsphere molecular junctions to electronically characterize the interaction between toxic gases and self-assembled monolayers. The metal-molecule-metal structures fabricated using this approach was used to study the adsorption of gaseous agents into highly ordered, well-defined two dimensional arrays of molecules incorporating known chemical functionality. The specific molecules chosen for our study included reactive chemical groups which mimic biological environments or capable of inducing transformations in the toxic agents penetrating the film. Molecules incorporating hydroxyl, carboxylic acid, amines, and transition-metal organometallic compounds were examined due to their potential reactivity with organosulfur and organophosphorous compounds. Measured changes in charge transport coupled with vibrational spectroscopy was used to perform an analysis of adsorption, retention, and interaction within a variety of engineered molecular environments with controlled structure and chemical functionality chosen specifically for their reactive nature with toxic compounds. The use of microsphere molecular junctions as a tool to examine chemical agent interaction with specific chemical functionalities on the nanoscale will provide information currently unavailable to the research community and help establish potentially useful technologies for chemical threat reduction.

Technical Report:

From October 1, 2007 through March 31, 2008, this program began by assembling the equipment and chemicals needed to carry out the research. The most critical component purchased and assembled during this period was the inert atmosphere glovebox system (total cost $23,140) which would house SAIC's Varian FT-IR Spectrophotometer fitted with a PIKE reflectance accessory. Although this instrument has been shown to function well for the study of

organic self-assembled monolayers on gold, trace amounts of atmospheric water and carbon dioxide in the purge gas was found to generate IR absorbances which interfered with the analysis of chemical interactions within a SAM. In order to completely remove all spectral interference from trace amounts of atmospheric water and carbon dioxide, we purchased a Vacuum Atmospheres Inert Glovebox system to house the FT-IR spectrophotometer and perform detailed chemical analysis on SAMs under controlled and inert environmental conditions. Figure 4 displays illustrations of the Varian FT-IR and glovebox purchased for this research program. This equipment will allow SAIC to perform detailed IR analysis of our SAMs under inert nitrogen atmospheres with oxygen and water contamination maintained below 0.1 ppm. This highly stable and inert environment will permit high resolution FT-IR analysis of our functionalized monolayers before and after exposure to toxic gases.

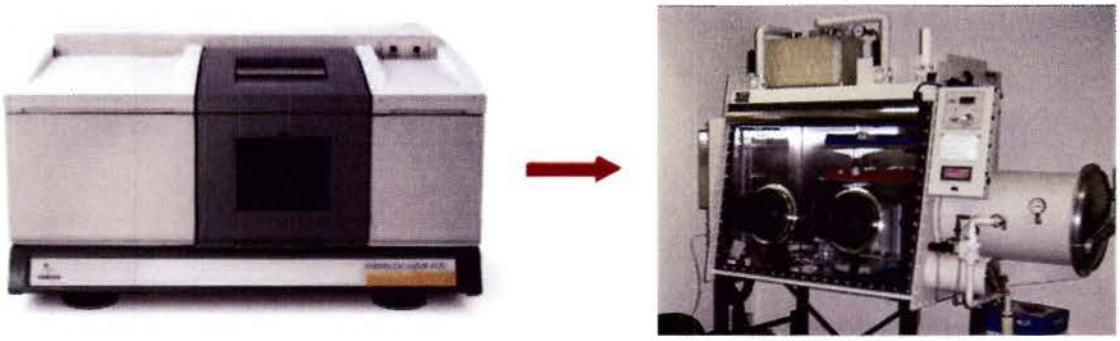

Figure 4. Image showing SAIC's Varian FTIR Spectrophotometer. In order to maximize the results achieved with this instrument for observing chemical interactions within self-assembled monolayers, the FT-IR was placed inside the inert nitrogen atmosphere of a Vacuum Atmosphere glovebox maintained below 0.1 ppm oxygen/water (shown at right).

Delivery of the nitrogen glovebox was made to our facility in Manassas, VA on January 30, 2008. The glovebox was immediately fitted with the components making it suitable for our requirements. Figure 5 shows images of the completed glovebox/FT-IR system assembled for this project. Access to the FT-IR and sample stage is achieved via the glove ports on the faceplate of the glovebox. Samples composed of self-assembled monolayers on gold-coated silicon (approximately 1×2 in.) are pumped into the glovebox using the antechamber on the right side of the glovebox and placed on the sample stage pictured in Figure 5c. After placement on the stage, control of the FT-IR is achieved using the external computer which is connected to the

instrument via a sealed electrical feed-through. Initially, and for a period of several weeks, out-gassing was observed from the interior of the IR spectrophotometer. High purity nitrogen was used to purge the interior of the instrument until the composition of the atmosphere had stabilized. Monitoring this process was readily achieved by simply observing the absorption spectra from a clean gold substrate. Over this period of time the levels of water and carbon dioxide dropped until spectroscopically negligible. After an inert atmosphere was achieved with the system, analysis of monolayers began.

Figure 5. a & b) Images showing SAIC's Varian FTIR Spectrophotometer inside the inert atmosphere of a Vacuum Atmosphere glovebox maintained below 0.2 ppm oxygen/water. **c)** Image showing the open sample chamber and PIKE specular reflectance accessory. SAM-functionalized substrates are placed over the open window on the reflectance stage to acquire IR data from the surface-attached monolayer.

To test the newly assembled inert atmosphere FT-IR, we examined the IR spectrum of a commonly used alkanethiol on gold. We deposited dodecanethiol (HS-C12) onto a freshly prepared gold substrate. After cleaning the gold surface, the substrate was immersed for 24 hrs. in a 1 mM ethanol solution of dodecanethiol. After surface functionalization, the substrate was briefly sonicated in ethanol to remove surface contaminants, followed by transferring the sample to the glovebox. A total of 1000 scans were collected at an angle of 80° using p-polarized light. Figure 6 shows the FT-IR spectrum of this film from 3000 to 2800 cm^{-1}. Shown are the prominent C-H stretching modes associated with the CH_2 and CH_3 groups of the hydrocarbon chain of the dodecanethiol. The location of the $CH_{2\ (as.)}$ mode observed at 2920 cm^{-1} also confirms the monolayer has a high degree of order as expected of a long alkanethiol on gold.

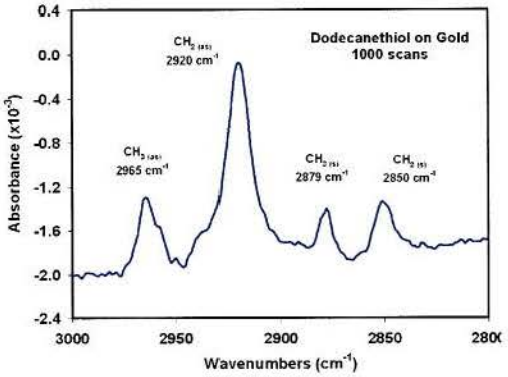

Figure 6. Surface reflectance FT-IR analysis of a Dodecanethiol (C-12) self-assembled monolayer on gold. 1000 scans were collected at 80° using p-polarized light.

After bringing the newly assembled glovebox/FT-IR system online, only negligible amounts of water and CO_2 were observed in the nitrogen atmosphere of the instrument. However, additional tests indicated that there were high levels of hydrocarbon vapor in the glovebox atmosphere. As shown in Figure 7, volatile hydrocarbons were found to quickly adsorb onto clean gold surfaces inside the glovebox atmosphere. The peaks observed at 2961 cm^{-1}, 2924 cm^{-1} and 2854 cm^{-1} are consistent with the C-H stretching bands of CH_2 and CH_3 groups from the volatile components of pump oil. The magnitude of these C-H stretching vibrational modes was at least comparable to those of SAMs formed from common alkanethiols on gold. The source of these contaminants were determined to be coming from the glovebox auxiliary vacuum pump, which normally operates continuously for maintaining a constant pressure within the glovebox and for evacuating the antechamber when transferring samples in and out of the box. To resolve this issue, the vacuum pump was replaced with an oil-free unit to eliminate the source of contamination. In addition, a cold trap was added in the vacuum line to further eliminate the hydrocarbon vapor and activated carbon was placed inside the glovebox atmosphere to remove the residual hydrocarbon from the glovebox atmosphere. These measures were found to be effective as shown in Figure 7b. Judging from the intensities of C-H absorption bands, a significantly lower level of contamination adsorbed onto the gold surface even after 24 hours. Within the timeframe of obtaining a spectrum (a few hours), the amount of contaminants that accumulated on the gold surface were kept insignificant.

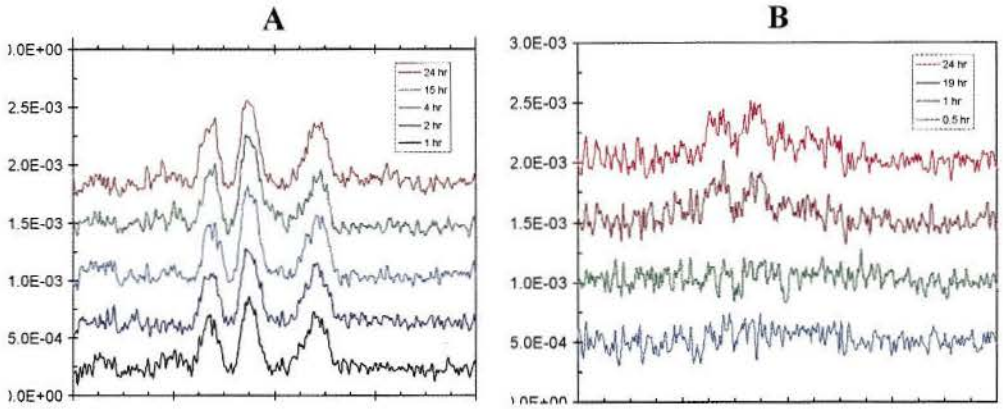

Figure 7. Accumulation of hydrocarbon contaminant from the glovebox atmosphere on a clean gold surface monitored by a series of infrared spectra recorded over time with **(A)** and without **(B)** the presence of activated carbon in the atmosphere.

During the period from April 1, 2008 to September 30, 2008, our research focused on characterizing functionalized thiols using the inert-atmosphere FT-IR system established in our laboratory. One functionalized alkanethiol we examined is 16-mercaptonhexadecanoic acid (MHA). The chemical structure of MHA is shown in Figure 8. A self-assembled monolayer of MHA was deposited onto a gold substrate by soaking in a 2 mM of MHA/ethanol solution overnight. The IR spectrum of the MHA monolayer on gold was obtained using a polarized incident infrared beam set at an angle of 80°. The FT-IR spectrum obtained from the MHA SAM is shown in Figure 9a. The prominent vibrational modes at 2851 cm^{-1} and 2920 cm^{-1} arise from the symmetric and asymmetric stretching modes of CH_2 contained in the MHA backbone. Note that no vibrational modes associated with CH_3 groups are present in the spectrum as expected. In addition, the features at 1700 cm^{-1} and 1460 cm^{-1} can be assigned to carboxylic acid C=O stretching and CH_2 scissors deformation respectively, and the absorption band at 1425 cm^{-1} is believed to be a combination of C–O stretch and C–O–H bending. These features confirm the assembly of MHA on the gold surface. Subsequently, we proceeded to examine the chemical interaction of MHA with chemical warfare agent simulants. The organophosphate compound, diethyl-chlorophosphate (DECP), was introduced to the MHA SAM. The exposure was carried out by placing the gold-MHA SAM in a sealed container that had a few drops of pure DECP at the bottom. The MHA SAM was exposed to the DECP vapor in the containers headspace for 1 hour. The physically adsorbed DECP was rinsed off the SAM surface with anhydrous ethanol, dried with N_2 stream and subsequently placed on the sample stage inside the spectrometer. The

spectrum of MHA after exposure to DECP is shown in Figure 9b. The most notable change in the MHA spectrum resulted from the exposure to DECP was a decrease in peak intensity for the vibrational mode at 1425 cm^{-1} as indicated by the arrow. As discussed earlier, the 1425 cm^{-1} contains substantial C–O–H bending character. A decrease in this particular vibrational mode suggests the cleavage of the proton off MHA. It's thus likely that the phosphorus group on DECP interacts with the carboxylic group on MHA, forming a ···COO–PO_3··· bond, with HCl as the byproduct of the reaction.

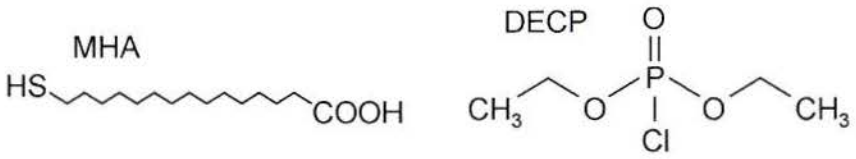

Figure 8. The chemical structures of 16-mercaptonhexadecanoic acid (MHA) and diethyl-chlorophosphate (DECP).

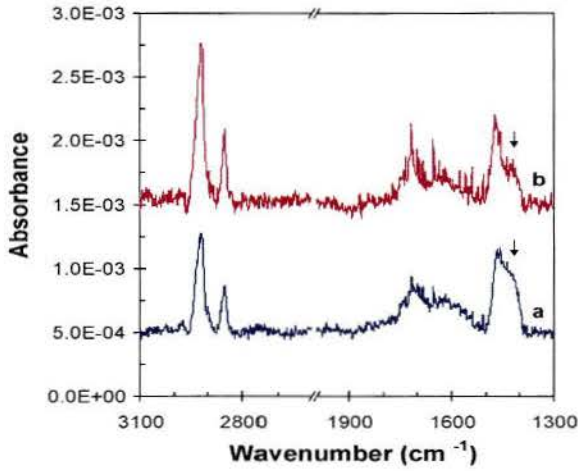

Figure 9. Infrared spectra for 16-mercaptonhexadecanoic acid **(a)** before and **(b)** after exposure to diethyl-chlorophosphate. Note that the spectra have been offset for clarity.

Scheme I

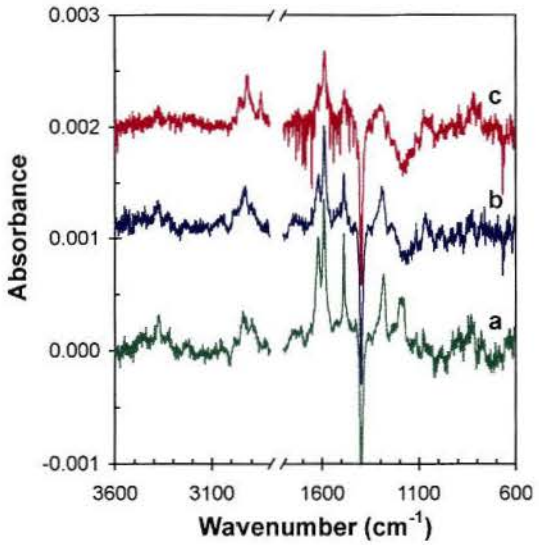

Figure 10. Infrared spectra of a 4-aminothiophenol SAM before **(a)** and after **(b)** exposure to DECP/ethanol and **(c)** DECP/H_2O/Ethanol. Note in Scheme I, the reaction between a terminal amine and 2-chloroethylethylsulfide results in the covalent linkage of the sulfide molecule to the terminal amine functionality with the formation of one equivalent of HCl as a byproduct and the loss of N-H groups on the amine.

In addition to the molecules discussed above, thiol molecules with hydroxyl (-OH) and amino (-NH_2) groups were also examined. Similar procedures were used to form the monolayers on gold by immersing the substrates in ethanol solutions of the molecules with concentrations between 1-2 mM for 24 hours. The resulting self-assembled monolayers were then characterized using reflectance FT-IR spectroscopy, and exposed to the chemical warfare agent simulants diethyl-chlorophosphate (DECP) and 2-chloroethylethylsulfide (CEES), followed by additional IR analysis to determine changes in the SAM. Results from the thiol incorporating the terminal amino group suggested the molecule forms high-quality monolayers. Figure 10a shows the infrared spectrum of a surface-attached monolayer of 4-aminothiophenol (4-ATP) on gold. Three characteristic absorption bands of the phenyl ring are well resolved at 1619, 1590, 1487 cm^{-1}, with a small absorbance observed at ~3400 cm^{-1} indicative of N-H stretching vibrations. After being exposed to DECP by soaking in DECP/ethanol solution, no change in the infrared spectrum was evident (Figure 10b). However, adding a small amount of water into the

DECP/ethanol mixture facilitates the chemical reaction between the 4-aminothiophenol monolayer and DECP. As shown in Figure 10c, a decrease in peak intensity of the N-H stretching vibration suggests the loss of the proton from the amine group. Similar to the interaction between the DECP and carboxylic groups, 4-aminothiophenol forms N-PO_3 bonds with the phosphate group in DECP. In addition, the linkage of the phosphate group to the amino group on 4-aminothiophenol alters the conjugation in the phenyl ring as shown in Figure 10c. Among the three ring vibration modes, only the mode at 1590 cm^{-1} remains. Further tests with another chemical warfare agent simulant, CEES, demonstrated similar changes in the IR spectra. Exposure to the more volatile CEES overnight induced sufficient change that the effect can be probed using IR.

The results discussed above clearly suggest that a promising candidate for nanoelectronic analysis was the molecular monolayer incorporating 4-aminothiophenol due to incorporation of highly reactive amino functionality. This is advantageous since in biology compounds such as mustard gas (bis(2-chloroethyl) sulfide) target the guanine nucleotide in DNA strands which also incorporate amine-terminated aryl groups. Mustard gas readily eliminates chloride ion by intramolecular nucleophilic substitution to form a cyclic sulfonium ion. This very reactive intermediate tends to bond to the pendant amine groups in DNA, which is particularly detrimental to cellular health and can lead to either cellular death or cancer. For this research project, pendant amine groups present on the surface of deposited self-assembled monolayers were expected to rapidly bind to incoming molecules of diethyl-chlorophosphate (DECP) or 2-chloroethylethylsulfide (CEES) causing an immediate and measurable change in the conductivity of molecular junctions incorporating these monolayers.

To test this theory, we fabricated a set of microsphere junctions incorporating 4-aminothiophenol. Since this particular molecular system is small in physical size when compared to other molecules (such as lengthy alkane thiols) it was possible that use of a 4-ATP monolayer may lead to electrical shorting of the device structure during fabrication. It has been known to us that use of "small" thiol molecules can lead to shorting of fabricated devices due to the incoming microsphere crushing through insufficiently thick SAMs which are unable to

withstand the magnetic deposition process. This results in the formation of metal-metal contacts through the organic monolayer and electrical shorting during analysis. In order to prevent this possibility, we decided to examine microsphere junctions which incorporate two SAMs by depositing self-assembled monolayers of 4-aminothiophenol on BOTH the surface of the magnetic arrays AND the surface of the metalized microspheres. Magnetic entrapment of the SAM-functionalized spheres onto SAM-functionalized arrays would then lead to molecular junctions with the theoretical structure as depicted schematically in Figure 11. In essence, nanoscale devices composed of [Gold-SAM-NH_2/NH_2-SAM-Gold] would be fabricated for electron transport analysis. Although, this picture is highly simplified since atmospheric water would also be strongly bound to the amino groups within each device and must be taken into consideration when determining the chemical mechanisms altering device conductance. The final nanoscale device as depicted in Figure 11 could then be exposed to a variety of chemical environments in order to measure the changes which occur to the electron transport through the Gold-SAM-NH_2/NH_2-SAM-Gold junction.

Fabrication of the devices were undertaken by depositing 4-aminothiophenol on both the magnetic arrays and magnetic microspheres. Deposition of the SAM on the gold-coated magnetic arrays utilized 1 mM ethanol solutions of 4-aminothiophenol degassed with argon. SAM deposition was allowed to proceed for 20 hrs. before rinsing the array with fresh ethanol and briefly sonicating the devices before drying then under a stream of nitrogen gas. Deposition of the 4-aminothiophenol SAM on the surface of the microspheres was again performed in approximately 1 mM ethanol solutions of the free thiol which also included a dispersion of the metalized microspheres. Since the micron-scale silica spheres settle out of solution over a period of hours, the mixture was periodically sonicated and shaken over 20 hrs. in order to fully functionalize the microspheres in the solution. After SAM formation, the microspheres were deposited onto the SAM-functionalized arrays to fabricate dual-monolayer nanoscale junctions. Entrapment of the magnetic microspheres was performed using a 250 G external magnetic field aligned parallel with the long axis of the devices in the array to promote domain alignment and formation of intense magnetic field strength in each device. Magnetic entrapment was performed for 30 minutes. After deposition of the microspheres, each array was then examined

under a high-power optical microscope to determine the location of each successful device. The completed arrays were then transferred to SAIC's Desert Cryogenics vacuum probe-station for electron transport analysis.

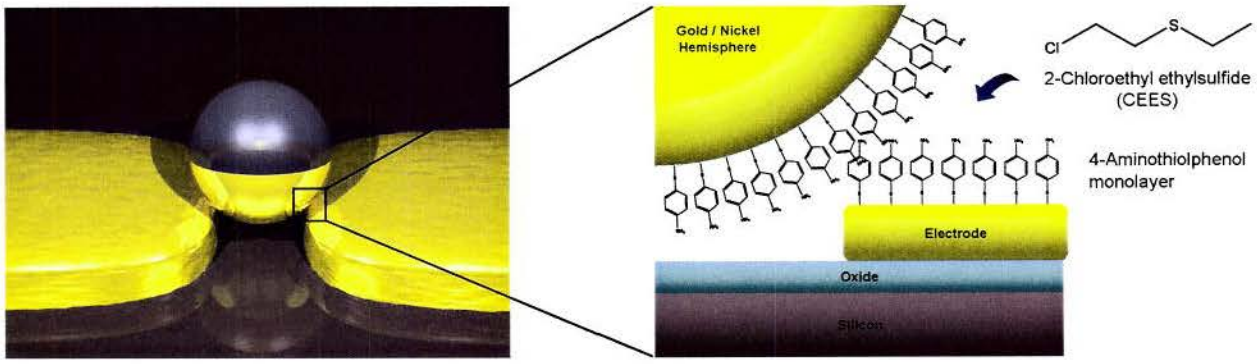

Figure 11. Illustration showing the structure of the molecular junctions produced when monolayers of 4-aminothiophenol (4-ATP) are deposited on BOTH the surface of SAIC's magnetic arrays and the metalized microsphere. After magnetic entrapment of the sphere, both SAMs are brought into contact with each other forming a layered [Gold-SAM-NH_2/NH_2-SAM-Gold] molecular junction for analysis.

In order to perform electron transport analysis of our nanoscale devices in a "real world" environment we did not initially place our devices under high vacuum or inert (argon) conditions as is typically done in the field of molecular electronics for device analysis. We instead performed an initial current-voltage analysis (I-V) on our devices under normal atmospheric conditions. Consequently, our devices incorporated extensive hydrogen bonding of water molecules at the amino interface within the molecular junctions. This would allow water molecules to act as proton transfer agents during reaction between the functionalized SAM and vapor-phase CEES molecules. Also, since the biological activity of CEES and other CWA simulants occurs in an aqueous environment in living tissue, performing our experiments in air was the preferred method rather than under controlled anhydrous conditions. Our electron transport analysis of 4-aminothiophenol was therefore conducted in the air to acquire transport data under ambient conditions. Following these measurements, the stage holding the magnetic array of 4-aminothiophenol junctions was removed from the probe-station and placed in a sealed chamber where a vapor of CEES molecules was developed, again all exposures were conducted in air. On the next day the stage was returned the probe-station and the devices once again measured. This transport data could then be directly compared to the conductivity of the same

devices before exposure in order to determine the influence CEES has on 4-aminothiophenol molecular junctions. The devices were then pumped down to high vacuum conditions to attempt removal of unbound molecular species in the junctions and again measured.

The results of these measurements are shown below in Figures 12 and 13. In all devices, I-V data acquired in air is plotted in blue, I-V data acquired after exposure to CEES vapor is shown in red, and I-V data acquired after exposure to vacuum is shown in black. In all devices a similar behavior was observed (see Figure 13). Initial I-V measurements of 4-aminothiophenol microsphere junctions in air were found to yield approximately 0.5 – 1.0 nA current at 100 mV bias. (Note, this value reflects the influence of water molecules hydrogen bound within the film and can not be thought of as the conductivity of the organic monolayers alone) After exposure in air to CEES vapor, all devices were found to display a pronounced loss in conductivity and can be explained by the reaction of the simulant at the amino functionality. Binding of CEES molecules within the 4-aminothiophenol junctions would disrupt contact between the two monolayers and hinder electron transport across each device. The infrared analysis discussed above for Figure 10 supports this conclusion by the observed loss of the N-H stretching frequency at 3400 cm^{-1} which is predicted from the chemical reaction proposed in Scheme I and by changes in the ring modes at 1597 and 1506 cm^{-1}. After exposure to vacuum, all devices were found to increase in overall conductivity and is likely due to dehydration of the junctions through the removal of water bound at the amino interface. These results demonstrate the sensitivity of molecular junctions to changing environmental and chemical conditions. Our work suggests amino-terminated monolayers may yield the most useful and sensitive molecular systems due to their high reactivity with a wide variety of toxic agents and similarity to biological systems.

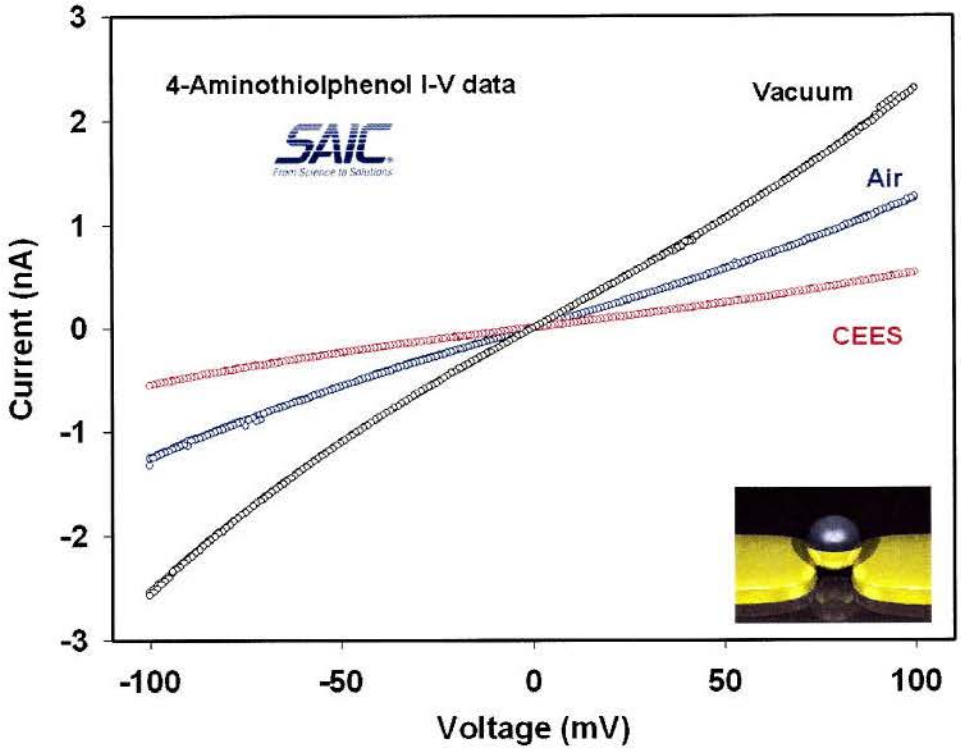

Figure 12. Electron transport characteristics of 4-aminothiophenol (4-ATP) under varying atmospheric conditions and after exposure to chloroethylethylsulfide (CEES). The changing transport characteristics suggest chemical interactions taking place within the molecular junctions alter the conductivity of the molecular conductor. Shown is I-V data from one device which was exposed to air, CEES vapor, and high vacuum conditions.

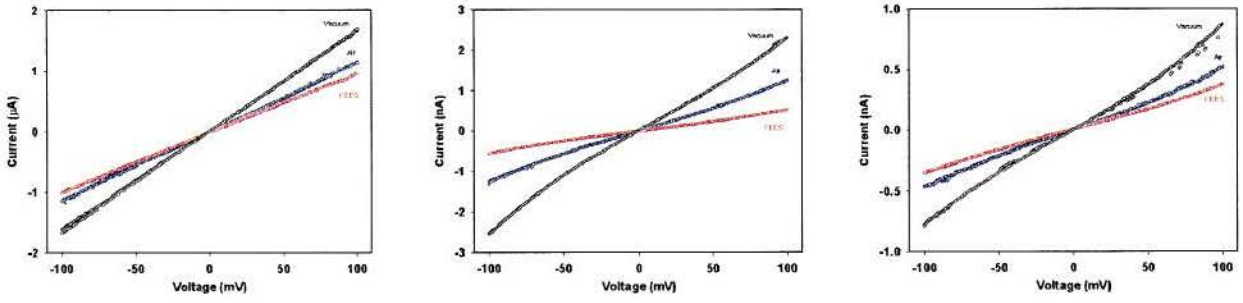

Figure 13. Electron transport characteristics of three different microsphere junctions incorporating 4-aminothiophenol under varying atmospheric conditions and after exposure to chloroethylethylsulfide (CEES). The similar conductance and changing electron transport patterns after exposure to different chemical environments suggests the behavior is the result of chemical interactions occurring within the 4-ATP SAMs.

Given the success of our spectroscopic and nanoelectronic analysis on molecular junctions incorporating 4-ATP, we continued during October to December 2008 examining this system using a variety of chemicals in order to better gauge the overall electrical response from this particular monolayer. Analysis of fabricated 4-ATP junctions were next performed by placing all devices under high vacuum conditions (1×10^{-6} torr) overnight. This procedure eliminated interference from bound water molecules in the SAM. On the following day, all devices were tested using SAIC's parametric analyzer to acquire baseline I-V data on 4-ATP monolayers under high-vacuum conditions. Typically, our devices were found to conduct approximately 100-300 nA of current at 100 mV bias. After these initial measurements, the probe-station was then backfilled with a variety of gases and chemicals, followed by additional current-voltage measurements in order to observe the changes each gas would have on the conductivity of the molecular junctions. Figure 14 displays a set of data from one microsphere junction incorporating two monolayers of 4-ATP. We began analysis by filling the probe-station with high-purity argon to atmospheric pressure and room temperature. Argon, being an inert gas was not expected to alter the conductivity of the 4-ATP junctions since interaction with the terminal amino-functionality was unlikely to occur. As expected, junctions incorporating 4-ATP showed little change in conductivity when devices were exposed to an atmosphere of pure argon. This control experiment also indicated that the change in pressure from high vacuum conditions to atmospheric pressure has little effect on the overall conductivity of our devices.

After exposure to inert gases, we again placed our 4-ATP microsphere junction under high-vacuum conditions in preparation for the next exposure. Since 4-aminothiolphenol is deposited in ethyl alcohol we next examined anhydrous EtOH (100 %). Ethanol was introduced to our devices by refilling the evacuated probe-station from a bubbler containing anhydrous EtOH. Argon was used as a carrier gas to introduce the vapor at room temperature. As can be seen in Figure 14a, ethanol/argon vapor is found to reduce the conductivity of the 4-ATP from 150 nA to approximately 120 nA at 100 mV bias. This decrease in conductivity was found to be fully reversible by reintroducing a high vacuum and is likely the result of non-covalent hydrogen-bonding between the –OH groups of the alcohol molecules and the $-NH_2$ groups within the 4-ATP SAM. This result, although fundamental, can be seen as vital since it

demonstrates that non-bonding interactions between gaseous molecules in the environment and functional groups within a self-assembled monolayer can also alters charge transport through a molecular junction sufficiently to be measured using electronic techniques. In this case, hydrogen-bonding between the alcohol molecules and the amino groups is sufficiently strong to cause a 20% drop in conduction through the film. We next examined ethyl alcohol which also contained 30% methyl amine ($MeNH_2$). Exposure of our evacuated 4-ATP junctions to this vapor was found to cause an immediate drop in conductivity from 150 nA to approximately 86 nA at 100 mV bias. This more pronounced loss in conductivity (42%) is due to the presence of the highly polar methyl amine molecules which can hydrogen-bond to the amino functionality in the 4-ATP SAM more strongly than the ethyl alcohol vapor alone. Again this effect was found to be reversible under vacuum suggesting the interaction, although stronger, is still non-covalent in nature and likely due to hydrogen bonding interactions with the film.

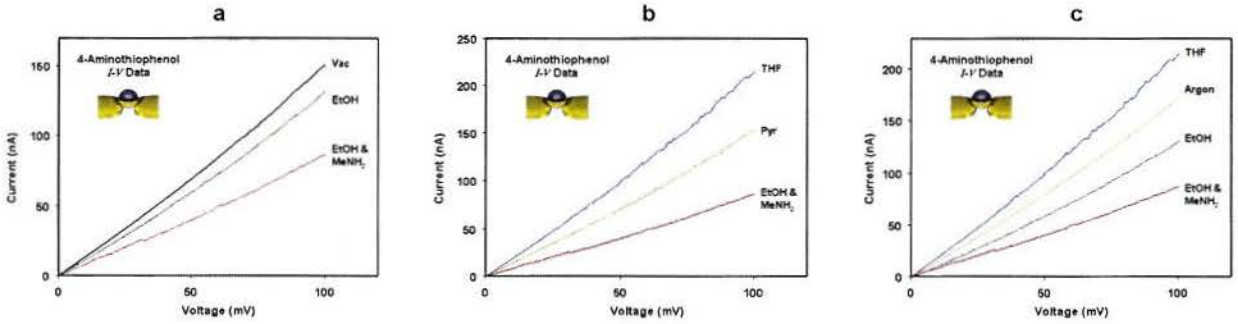

Figure 14. Current-voltage properties of 4-aminothiolphenol (4-ATP) molecular junctions under a variety of chemical atmospheres. Plots presented as the average of the forward and reverse traces. **a)** I-V properties of 4-ATP molecular junctions exposed to vacuum (black), ethyl alcohol (green), and ethyl alcohol/30% methyl amine (red) vapor at 1 atmospheric pressure and 25 C. **b)** I-V properties of 4-ATP molecular junctions exposed to tetrahydrofuran (blue), pyridine (gold), and ethyl alcohol/30% methyl amine (red) vapor at 1 atmospheric pressure and 25 C. **c)** I-V properties of 4-ATP molecular junctions exposed to tetrahydrofuran (blue), argon (orange), ethyl alcohol (green), and ethyl alcohol/30% methyl amine (red) vapor at 1 atmospheric pressure and 25 °C.

Tetrahydrofuran (THF), a common solvent and cyclic ether, was also examined. THF was introduced to our devices as the pure vapor using a bubbler and argon gas. The effects measured on our 4-ATP microsphere junctions compared to other gases are shown in Figures 14b and 14c. Tetrahydrofuran was found to *increase* the conductivity of our devices from 150

nA under vacuum to approximately 220 nA at 100 mV bias. The observed change in current through our 4-ATP junctions is likely caused by strong interactions between the amine protons and the lone pairs of electron present on the Lewis-base ether functionality of THF. The observed increase in the SAMs conductivity rather than a decrease remains unexplained. One possible cause however, may be due to the formation of stabilized charges within the SAM. The formation of stable charges within the 4-ATP SAM could increase conductivity if electrons utilize these sites when tunneling through the molecule from the source to drain electrodes. This suggests that exposure of molecular junctions incorporating 4-ATP to THF vapor initiates new tunneling mechanisms since electron transport is typically the result of coherent "orbital mediated" tunneling unrelated to the "hopping" mechanisms found in electrically charged systems. This finding suggests the presence of chemical species inside molecular junctions can alter the mechanism of electron transport through a SAM.

Lastly, we also examined the common heterocyclic aromatic solvent pyridine. The choice to examine pyridine was based on the nitrogen heteroatom which features a strongly basic lone pair of electrons. Because this lone pair is not delocalized in the aromatic system, pyridine is very basic with chemical properties similar to tertiary amines. Pyridine can be protonated by reaction with acids and forms a positively charged aromatic polyatomic ion called a pyridinium cation. Unfortunately, although pyridine is known to be strongly nucleophilic in nature and expected to cause significant changes to the conductivity of molecular junctions, the high boiling point of pyridine (115 ^{o}C), prevented us from transferring significant quantities of the compound to our fabricated devices using an argon bubbler, thus limiting the observed effect. As a result, Figure 14b shows only minimal effect on the conductivity of the 4-ATP junctions after exposure to pyridine.

In addition to our examination of 4-aminothiolphenol molecular junctions, during this same period our research also focused on molecular SAMs composed of 4-mercaptobenzoic acid (4-MBA). This aromatic thiol is similar to 4-aminothiolphenol except 4-MBA incorporates a carboxyl functionality (-COOH) rather than amine in its terminal position. Deposition of high quality 4-MBA SAMs were confirmed using reflectance FT-IR on gold substrates. Our

reflectance spectra of 4-MBA are representative of fully protonated monolayers and are consistent with previously published spectra. The spectrum of 4-MBA shown in Figure 15 is dominated by ν(C=O) at 1742 cm-1. A shoulder at 1710 cm-1 is also visible. Recently it has been argued that these two transitions correspond to molecules that are unassociated (1742 cm-1) and associated (1710 cm-1) through hydrogen-bonding interactions within the layer. These interactions would almost certainly dominate the interface between two 4-MBA SAMs in close contact within a double microsphere junction after fabrication of microsphere junctions.

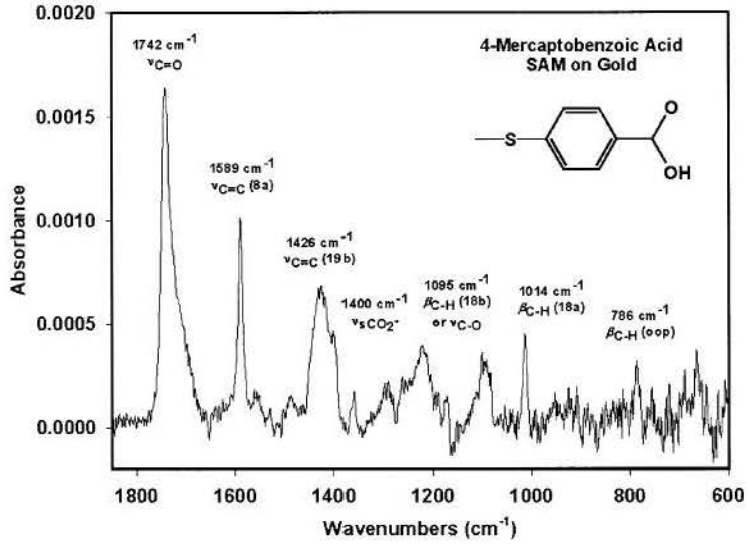

Figure 15. FT-IR analysis of a 4-mercaptobenzoic acid (4-MBA) self-assembled monolayer on gold. Major vibrational modes have been identified. The spectrum was acquired using 6000 scans from SAIC's Varian 3100 spectrophotometer equipped with a VeeMax-II variable angle specular reflectance stage and infrared polarizer. Our FT-IR is housed inside a Vacuum-Atmosphere glovebox maintained below 0.1 ppm contamination to eliminate all modes associated with water and carbon dioxide which do not appear in the above spectrum.

After confirming the formation of high-quality monolayers of 4-MBA on gold using FT-IR spectroscopy, we again turned to the microsphere test-bed to explore the reactivity of this system using molecular junctions. Once again, due to the small size of 4-MBA, we chose to fabricate junctions which incorporated two layers of the SAM in order to minimize electrical shorting of devices during fabrication. Deposition of the SAM on the gold-coated magnetic arrays utilized 1 mM ethanol solutions of 4-MBA degassed with argon. SAM deposition was allowed to proceed for 20 hrs. before rinsing the array with fresh ethanol and drying with

nitrogen gas. Deposition of the 4-MBA on the surface of the microspheres was performed in approximately 1 mM ethanol solutions of the free thiol which included a dispersion of the metalized microspheres. After SAM formation, the microspheres were magnetically deposited into the SAM-functionalized arrays to fabricate molecular junctions incorporating dual-SAM junctions as shown in Figure 11. The completed arrays were then transferred to SAIC's Desert Cryogenics vacuum probe-station for electron transport analysis.

Our initial analysis of 4-MBA examined the electrical response of this SAM on exposure to diethyl-chlorophosphate (DECP), a known simulant for organophosphate nerve agents. After fabrication, our devices were transferred to SAIC's Desert Cryogenics vacuum probe-station for electron transport characterization. Our 4-MBA molecular junctions were maintained under ambient atmospheric conditions in order to leave atmospheric water in place within the film and allow for a more realistic test with the CWA simulant. Under normal atmospheric conditions all devices were tested to record baseline I-V characteristics before exposure to the simulant. Current-voltage data collected on 4-MBA in air are shown for three separate devices in Figure 16 and illustrated in blue. Our measurements show typical current levels through 4-MBA microsphere junctions range from 30 and 60 nA at 100 mV bias. After recording baseline measurements in air, the sample stage holding the array of molecular junctions was removed from the probe-station and placed in a glass chamber which held a saturated vapor of DECP. Our devices were exposed to this simulant for exactly 5 hours before being removed and returned to the probe-station for analysis. Figure 16 displays the changes in electron transport through our devices illustrated in red. In all cases the measured current was dramatically reduced, typically by factors of 5 to 10. This effect is found to be approximately twice the effect recorded from 4-ATP with the half-mustard simulant CEES shown in Figure 12. The greater decrease in electron transport is likely due to use of a carboxyl functionality which incorporates a proton with higher acidity, increasing the likelihood of combining with the leaving group of the DECP to create a molecule of HCl.

The higher reactivity observed for 4-MBA with DECP implies chemical interactions taking place other than simple non-covalent hydrogen bonding. If true, then irreversible covalent

bond formation likely occurred, which would lead to loss of the carboxyl functionality within our molecular junctions. We attempted to confirm this by exposing our DECP-exposed devices to high vacuum for 20 hours in an attempt to remove all non-bonding molecules absorbed into the junctions. On the next day we then repeated our I-V measurements in order to compare with the previously acquired data. Figure 16 shows the results of these measurements as the I-V traces colored in black. In all cases we find our devices recover only slightly after removal of all non-bonded species from the films, implying irreversible chemical reactions have occurred between the 4-MBA carboxyl functionality and the DECP simulant. Although the exact cause of the minimal recovery is unknown, we believe the effect is most likely related to removal of associated water molecules from the carboxyl and gold-sulfur interfaces rather than elimination of bound DECP species. Our previous work has shown that thiol monolayers exposed to air quickly absorb atmospheric water molecules at the gold-thiol contacts in addition to other functionalities present in the SAM and can result in an increase of molecular conductivity if removed under vacuum. In the current case, since recovery of the 4-MBA / DECP junctions remained far below the initial baseline measurement acquired in air, we conclude that irreversible reactions have occurred between the SAM and the simulant which induced a dramatic decrease in molecular conductivity.

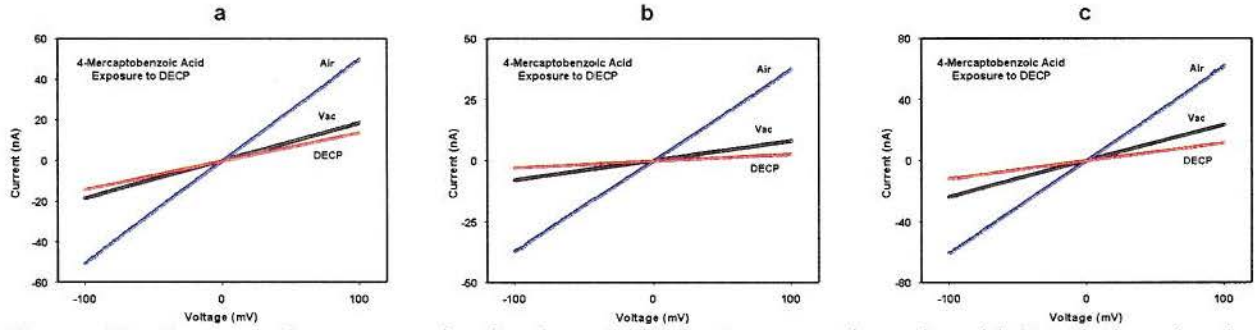

Figure 16. Current-voltage properties for three different 4-mercaptobenzoic acid (4-MBA) molecular junctions before and after exposure to diethyl-chlorophosphate (DECP). Plots are presented as the average of the forward and reverse traces. All devices were examined initially in air (blue), then following a 5 hour exposure to DECP vapor in air (red), and again after exposure to high vacuum conditions for 20 hrs. (black). All devices display the same pattern of intense conductivity loss after DECP exposure and minor recovery after vacuum, suggesting irreversible reactions have occurred.

To confirm covalent reactions, we examined self-assembled monolayers of 4-MBA using surface-reflectance FT-IR spectroscopy, the results of which are shown in Figure 17. For these measurements, gold substrates were fabricated using thermal evaporation. The silicon wafers

were coated with approximately 300 nm thick films of gold. Figure 17a shows the spectrum of 4-mercaptobenzoic acid which is dominated by a C=O stretch at 1742 cm^{-1}, phenyl ring stretching at 1589 cm^{-1}, and C-O stretching 1410 cm^{-1}. Upon exposure to either DECP (Figure 17b) or half-mustard (Figure 17c), a shoulder at 1710 cm^{-1} develops due to associated C=O. In addition, a substantial decrease in peak intensity can be observed with the 1410 cm^{-1} C-O stretch. However, no changes are observed with the phenyl ring stretching modes at 1589 cm^{-1}. The changes in IR spectra can be explained by the formation of a $-C_5H_4-COO^-$ anion when exposed to these simulants. The resonance effects in a carboxylate anion (*i.e.* the sharing of the negative charge between the two oxygen atoms) will result in each of the C-O bonds to have partial double bond character. These findings suggest that the loss a proton from the carboxyl group occurs, and likely that DECP or half mustard eliminates a chloride ion while reacting with the mercaptobenzoic acid at the C=O sites.

Additional research was also performed involving FT-IR spectroscopy of self-assembled monolayers composed of 4-mercaptophenol. Figure 18a shows the infrared spectrum of 4-mercaptophenol prior to agent exposure. The spectrum clearly reveals characteristic absorption bands of a phenol, with three vibrational modes of a phenyl ring at 1594 cm^{-1}, 1579 cm^{-1}, and 1487 cm^{-1}, along with the C-O stretch at 1266 cm^{-1}. Upon exposure to DECP, no apparent changes in the IR spectrum were observed (Figure 18b), suggesting that the hydroxyl group in a phenol were unreactive to the organophosphate compound over the time of agent exposure. However, noticeable changes in the IR spectrum could be seen when the 4-mercaptophenol SAM was exposed to half-mustard. As shown in Figure 18c, the relative strength of the absorption peaks at 1594 and 1579 cm^{-1} decreases while the absorption peak at 1487 cm^{-1} gains in intensity, indicating that the chemical interaction with half mustard has induced a conjugational change within the aromatic ring of the phenol. In addition, a blue shift of the C-O stretch from 1266 cm^{-1} to 1280 cm^{-1} is also evident. These observations seem to suggest the resonance stabilization of the phenoxide anion by the aromatic ring, as commonly observed in a phenol. However, due to background noise, it was difficult to distinguish the O-H stretch at ~3400 cm^{-1} in the IR spectrum. Although the cleavage of the proton off the hydroxyl group is to be expected upon

exposure to half mustard, we currently do not have direct experimental evidence to support that assumption.

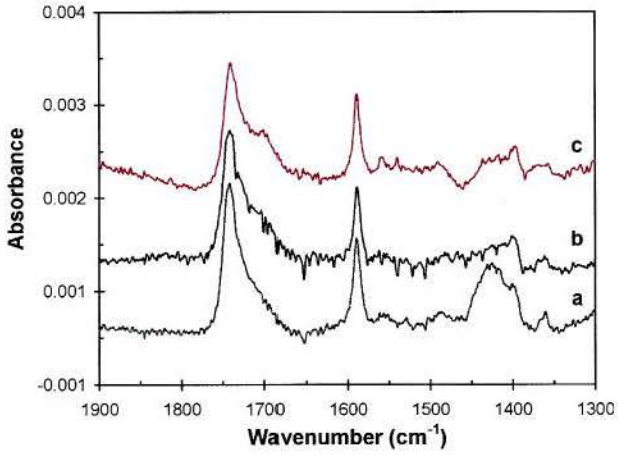

Figure 17. Infrared spectra of 4-mercaptobezonic acid SAMs. **a)** 4-MBA film after deposition on gold substrate. **b)** 4-MBA film after exposure to DECP. **c)** 4-MBA film after exposure to chloroethylethylsulfide (half mustard stimulant). Note that the spectra have been offset for clarity.

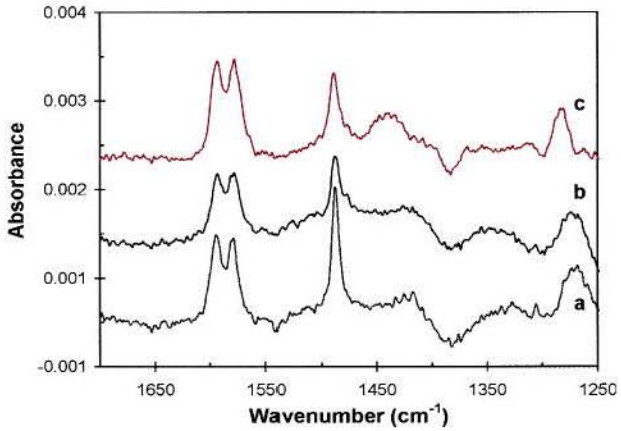

Figure 18. Infrared spectra of a 4-mercaptophenol SAM (a) before and after exposure to (b) DECP and (c) half-mustard. Note that the spectra have been offset for clarity.

During the period from December 2008 to July 2009 our research focused on a novel self-assembled monolayer based on a metal-organic framework (MOF). Metal-organic frameworks are an emerging class of crystalline material whose structure is made up of extended 3D networks of metal ions and multidentate organic ligands. These building units organize spatially in such a way that crystalline porous structures which define channels and cavities of regular size and shape on the nanometer scale are formed. MOFs have an extremely open

structure in which the free space available for host molecules can reach up to 90% of the crystal volume. The design and synthesis of metal-organic frameworks (MOFs) has yielded a large number of structures which have been shown to have useful gas and liquid adsorption properties. In particular, porous structures constructed from discrete metal carboxylate clusters and organic ligands have been shown to be amenable to systematic variation in pore size and functionality. The permanent porosity of MOFs is imparted by the structure of the metal-carboxylate clusters, where each metal ion is locked into position by the carboxylates to produce rigid entities of simple geometry as illustrated in Figure 19. The tunable nature of MOF materials, coupled with high internal void space makes these materials potentially useful for a variety of filtration, absorption, and sensing applications.

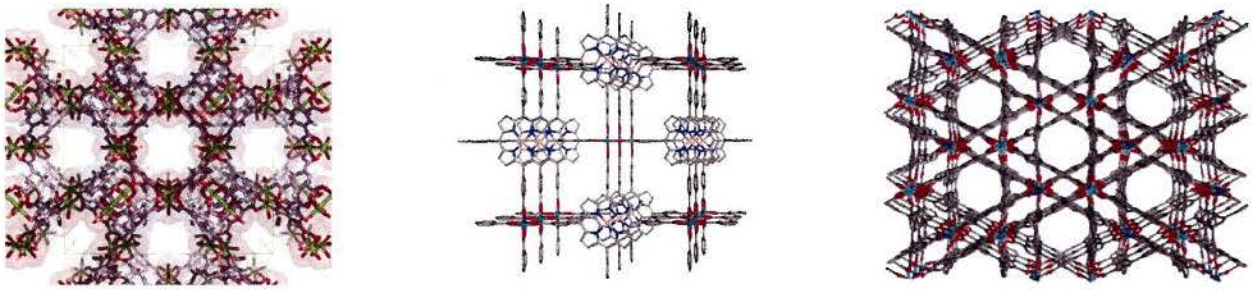

Figure 19. Molecular structures of various metal-organic frameworks. The regularly shaped nanoscale voids within the structures where gases and other guest molecules rapidly absorb are visible.

Recently, a copper-based MOF (known as HKUST-1) has been shown to be amenable to layer-by-layer deposition from ethanol solutions onto functionalized gold surfaces.[21] Thin-films of HKUST-1 on gold permit incorporation of the MOF into the microsphere test-bed for electrical analysis and monitoring of its conductivity. It has been previously shown that use of carboxy-terminated SAMs on gold could initiate formation of the HKUST-1 MOF structure when substrates were sequentially immersed in separate ethanol solutions containing copper (II) acetate and trimesic acid, (see Figure 20).[21] Single-crystal data have shown that this material forms face centered-cubic crystals that contain an intersecting three dimensional system of large square-shaped pores (9 × 9 Å), and that the MOF retains this structure on gold surfaces. Figure 20 displays representations of the MOF structure. In HKUST-1, Cu^{2+} ions form dimers, where each copper atom is coordinated by four oxygen atoms provided by the trimesic acid linkers and

by one water molecule. The presence of water molecules in the first coordination sphere of the copper ions leads to the possibility of opening a site on the copper through dehydration of the MOF, thus increasing the ability of HKUST-1 thin films to be used in molecular absorption applications or sensors. Studies have shown that removal of water molecules from HKUST does not alter the MOFs structure, allowing increased absorption of guest molecules.

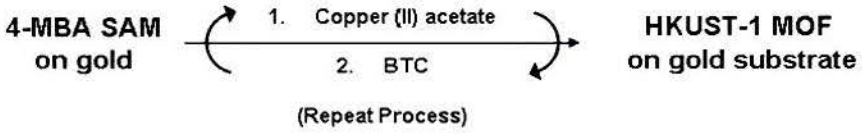

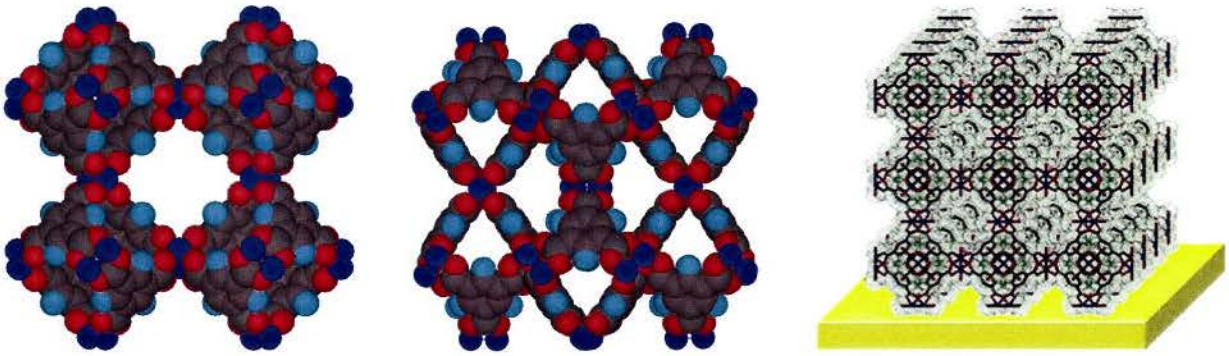

Figure 20. Deposition scheme for HKUST-1 on 4-MBA functionalized gold surfaces. Illustrations depict the crystal structure of the HKUST-1 framework. Note the regular voids within the MOF where gases and other guest molecules freely enter and bind into the structure.

Our research on MOF thin-films began by determining whether HKUST-1 could be grown from gold surfaces functionalized with thiol monolayers conducive for nanoelectronic measurements. We began by examining 4-mercaptobenzoic acid (4-MBA). This carboxy-terminated arylthiol (see Figure 15) is a small aromatic molecule which would yield a highly conductive organic SAM to link the MOF to the metal surface. In addition, the molecular structure of 4-MBA is very similar to trimesic acid (both incorporate single benzene rings with carboxy substituents) yielding a SAM which would become part of the HKUST-1 MOF thin-film, eliminating the electronic effects encountered when using a alkanethiol SAM. Use of 4-MBA would therefore allow detailed electron transport measurements of the MOF film. Figure 21 shows FT-IR analysis of our fabricated films. Figure 21a shows an example of a deposited 4-MBA film used to initiate growth of the MOF. The IR spectrum is dominated by an intense peak

at 1742 cm^{-1} due to the carbonyl stretching mode and was found to match well with literature results, suggesting a dense well-formed monolayer. Figure 21b shows the same film after exposure to one cycle of Cu (II) acetate followed by trimesic acid. After the first MOF cycle, the peak at 1742 cm^{-1} decreases in intensity as copper atoms bind to the surface carboxyls converting them to carboxylate groups (COO^-). Simultaneously, several new modes associated with the IR spectrum of HKUST-1 begin to appear (Figure 21b). In order to follow the growth of the HKUST MOF on our substrates and confirm layer-by-layer deposition, we performed surface-reflectance IR after every deposition cycle for a total of eight layers (Cu (II) acetate followed by trimesic acid = 1 cycle). Figure 22 shows the overlay of all IR spectra obtained during this process. Layer-by-layer growth of HKUST-1 is confirmed by the systematic increase in intensity of the vibrational modes associated with the framework as each cycle is deposited on the surface. Figure 22b shows a plot of the increase in absorbance of the largest mode at 1381 cm^{-1} as a function of the number of cycles deposited. The steady increase in absorbance confirms layer-by-layer growth of the HKUST-1 on 4-MBA functionalized substrates and demonstrates this technique allows for precise control over MOF-SAM thickness by simply controlling the number of layers deposited.

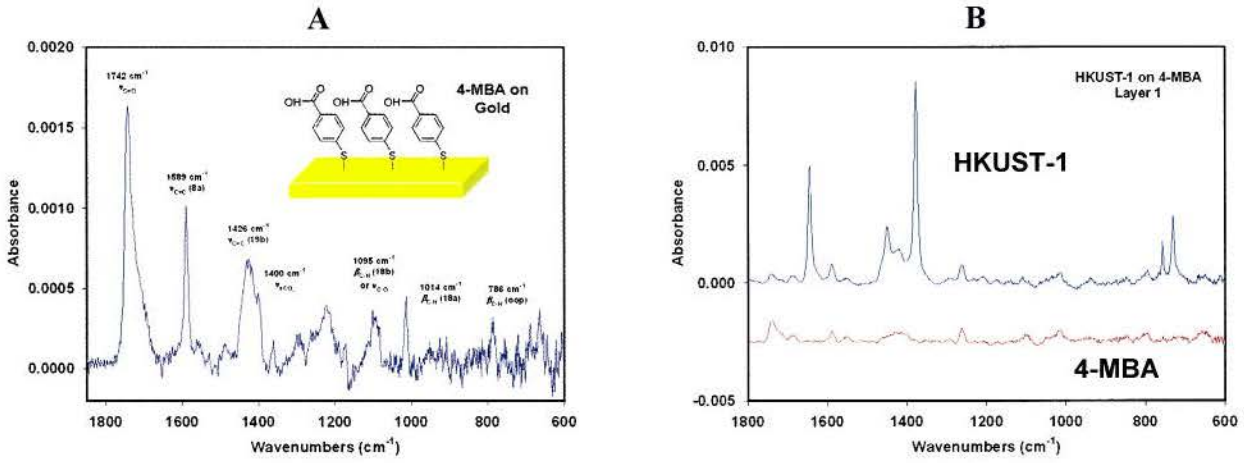

Figure 21. Surface-reflectance IR data showing **a)** 4-mercaptobenzoic acid (4-MBA) on a planar gold substrate, and **b)** the same substrate after immersion in copper (II) acetate in ethanol (1 mM, 30 min.) and trimesic acid in ethanol (1 mM, 30 min.). Red shows the 4-MBA SAM, while the blue spectrum shows the film after initial formation of the MOF.

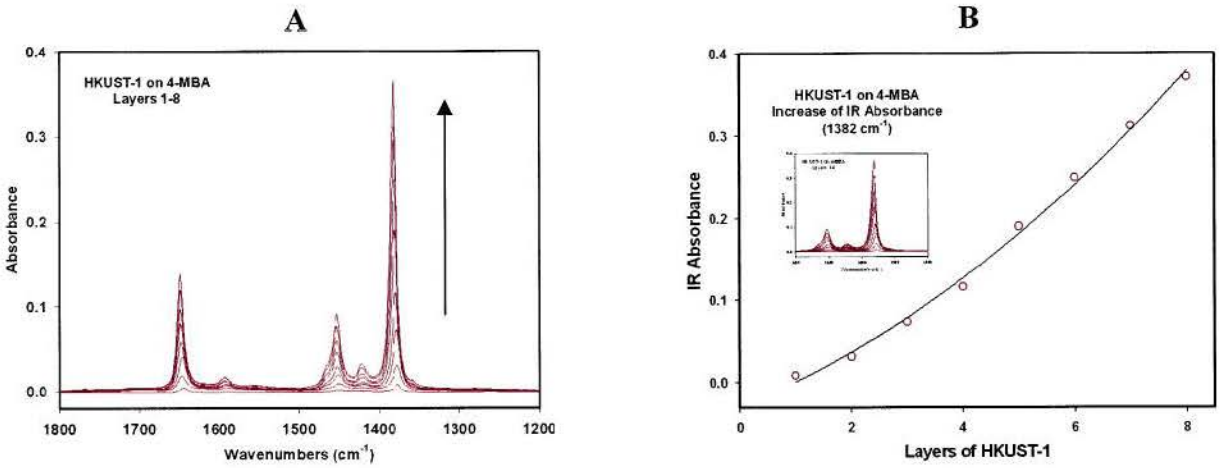

Figure 22. Surface-reflectance FT-IR acquired on a 4-MBA SAM on gold after each of eight cycles of copper (II) acetate and trimesic acid immersion. **a)** IR spectra from 1200 -1800 cm^{-1} showing the change in intensity of HKUST-1 vibrational modes after each cycle. **b)** Plot showing the increase in IR absorbance using the $\nu_s(COO^-)$ mode at 1382 cm^{-1} as a function of the number of cycles. These results confirm HKUST-1 deposits on 4-MBA functionalized gold surfaces in a stepwise layer-by-layer fashion.

Figure 23 displays the complete IR spectrum of HKUST-1 on gold initiated using a 4-MBA monolayer from 500 cm^{-1} to 1800 cm^{-1}. The spectrum is dominated by symmetric and asymmetric COO^- stretching modes appearing at 1381 cm^{-1} and 1649 cm^{-1} respectively, and brought about by the two modes of the COO^- functionality bound to the copper (II) ions. The inset of Figure 23 shows a peak found at 3097 cm^{-1} which is caused by aromatic ν(C-H) stretching vibrations from the benzene hydrogen atoms. In addition, modes observed at 758 cm^{-1} and 733 cm^{-1} arise from the (C-H) out-of-plane (oop) modes of these same protons. Lastly, a small mode observe at 514 cm^{-1} is due to direct Cu-O coupling and caused by ν(Cu-O) stretching vibrations. This mode, due to its direct bonding of the copper ions and the oxygen of the ligand confirms direct attachment of the metal to the trimesic acid. This mode would be expected to display the greatest change in frequency (red or blue shifts) as different organic molecules enter into the framework and bind at the open copper sites. Highly polar molecules (for example carbon monoxide or organophosphates) would be expected to shift the frequency of the Cu-O stretching mode considerably allowing for confirmation of binding of these molecules to the copper using IR spectroscopy. The spectrum displayed in Figure 23 matches that of HKUST-1 in the bulk phase suggesting thin-films of this material retains the ordered structure shown in Figure 20. This also suggests that our deposited films of HKUST-1 should incorporate the same

nanoscale voids and channels found in the bulk material. These nanoscale pores (approximately 1 nm across) should accommodate a wide variety of guest molecules including toxic industrial chemicals and CWA simulants studied under this program. Figure 24 shows SEM images of a HKUST-1 thin film on gold and illustrates the excellent coverage obtained using this technique. No defects or holes to the gold surface are observed. Using nanoscale films of HKUST-1 like these, we studied this material for its ability to absorb small organic molecules and how this absorption affects the electrical properties of the metal-organic framework.

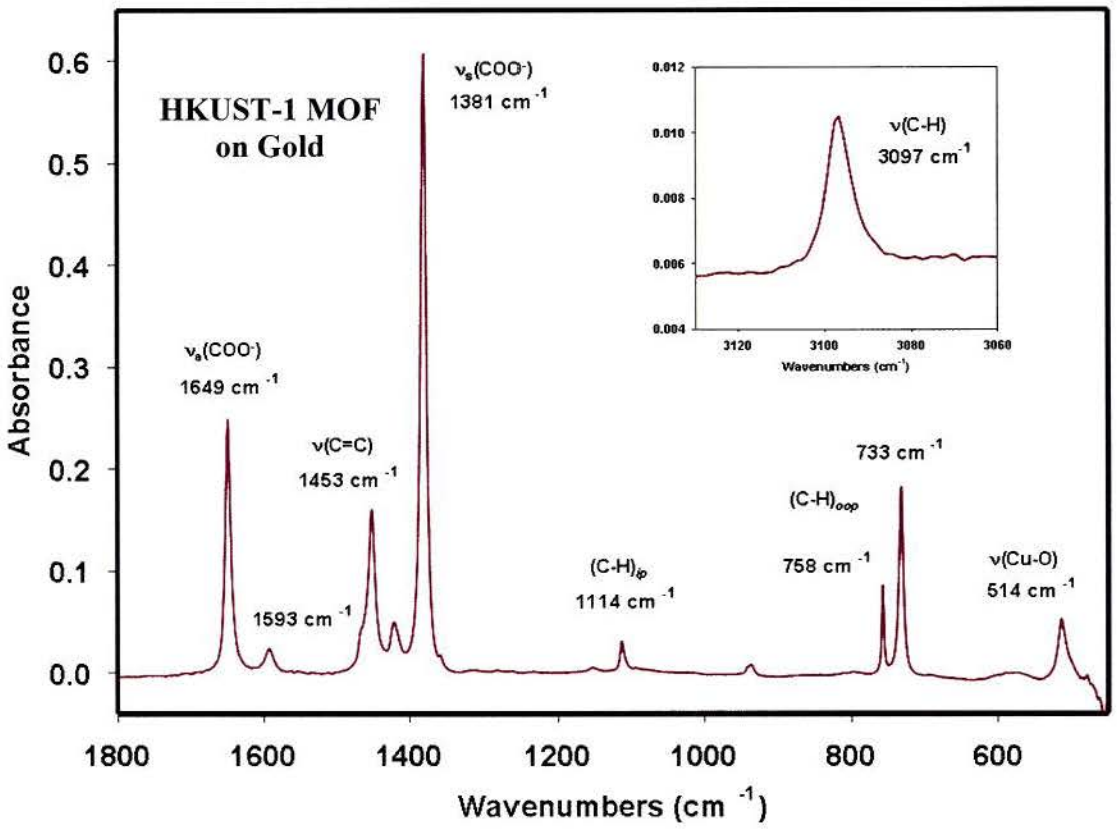

Figure 23. Complete FT-IR spectrum of HKUST-1 MOF on 4-MBA/gold substrate. Major peaks have been labeled to indicate frequency and the molecular vibration responsible for the absorption. Inset shows the peak found at 3097 cm^{-1} due to ν(C-H) stretching modes.

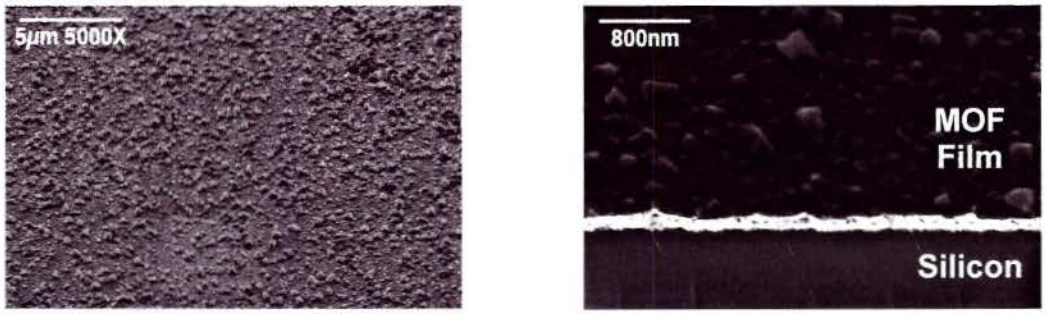

Figure 24. Scanning electron microscope (SEM) images of HKUST-1 MOF-SAM on a gold-coated silicon substrate.

Initially, we examined the ability of HKUST-1 to absorb a variety of toxic compounds of interest to DTRA. We first examined carbon monoxide which has been shown in the literature to absorb into the bulk HKUST-1 MOF. Our experiments utilized HKUST-1 which had been fully dehydrated under high vacuum conditions (1×10^{-6} torr) to remove all traces of water from the MOF. After dehydration, the MOF was exposed to carbon monoxide at 1 atm. pressure then returned to the FT-IR spectrometer for spectroscopic analysis. Figure 25 shows the result of this absorption experiment. Carbon monoxide is found to absorb into HKUST-1 to high concentration as evidence by the intense vibrational modes observed at 2000 cm^{-1} arising from C≡O stretching vibrations. Direct bonding of the carbon monoxide to open copper sites in the MOF is confirmed by the observation of a small peak at 640 cm^{-1} which arises from Cu-C≡O stretching on the metal. This peak is over 100 cm^{-1} higher in frequency compared to the ν(Cu-O) stretching mode of the framework. This significant blue-shift is due to "back-bonding" interactions between the carbon monoxide molecule and empty d-orbitals on the copper atom which acts to strengthen the bond between the copper and the bound ligand. Upon exposure to vacuum, all evidence of carbon monoxide can be removed from the MOF.

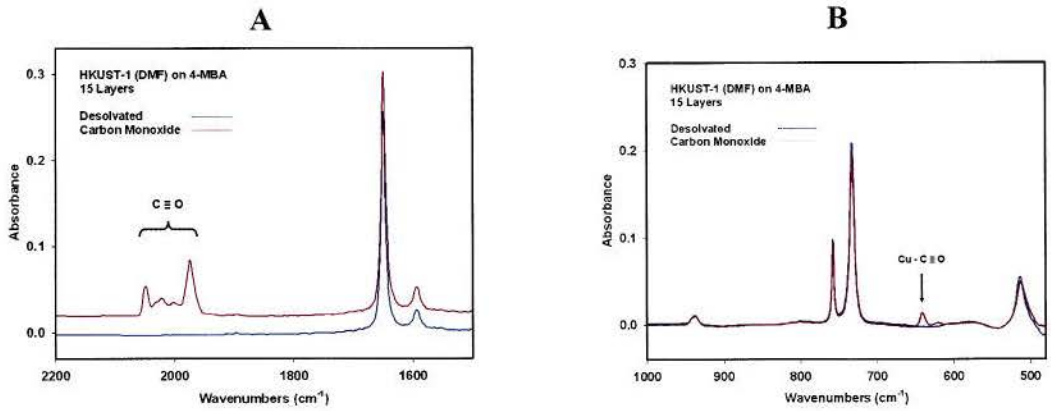

Figure 25. Reflectance FT-IR analysis of a HKUST-1 on gold after exposure to carbon monoxide. A significant concentration of CO absorbs into the MOF from the intensity of the peaks observed in the 2000 cm^{-1} region. Molecules of CO are found to bind directly to the open sites on the copper ions as evidenced by a peak at 640 cm^{-1} which is due to direct coupling of the gas to dehydrated copper atoms in the framework.

We also determined that larger organic molecules which incorporate cyano-functionality also have high affinity for the HKUST-1 framework, as illustrated in Figure 26. In these experiments, dehydrated HKUST-1 was exposed to ethanol solutions containing approximately 0.5 mM concentration of tetracyanoquinodimethane (TCNQ), the structure of which is illustrated in figure 26a. Similar to carbon monoxide, TCNQ was also found to absorb to high concentration in the MOF as evidenced by the intense cyano-stretching mode observed at 2200 cm^{-1} (several other vibrational modes associated with the molecule are also observed in the exposed HKUST-1 spectrum and are marked in Figure 26a). Evidence for direct coupling of TCNQ to dehydrated copper sites within the MOF was found in a small peak at 574 cm^{-1} attributed to a Cu-N≡C stretching mode between the nitrogen and copper. This peak is observed to lie much closer to the ν(Cu-O) stretching mode of the framework (514 cm^{-1}) as expected due to lack of back-bonding. This result suggests that despite incorporating relatively bulky structures, large organic molecules which contain strong donating functionality can rapidly absorb into the MOF. Attempts to study the absorption of several other organic molecules failed mainly due to a lack of strongly polar groups on their structure. Only low concentration of solvents such as ethyl ether and tetrahydrofuran were found to absorb into HKUST-1.

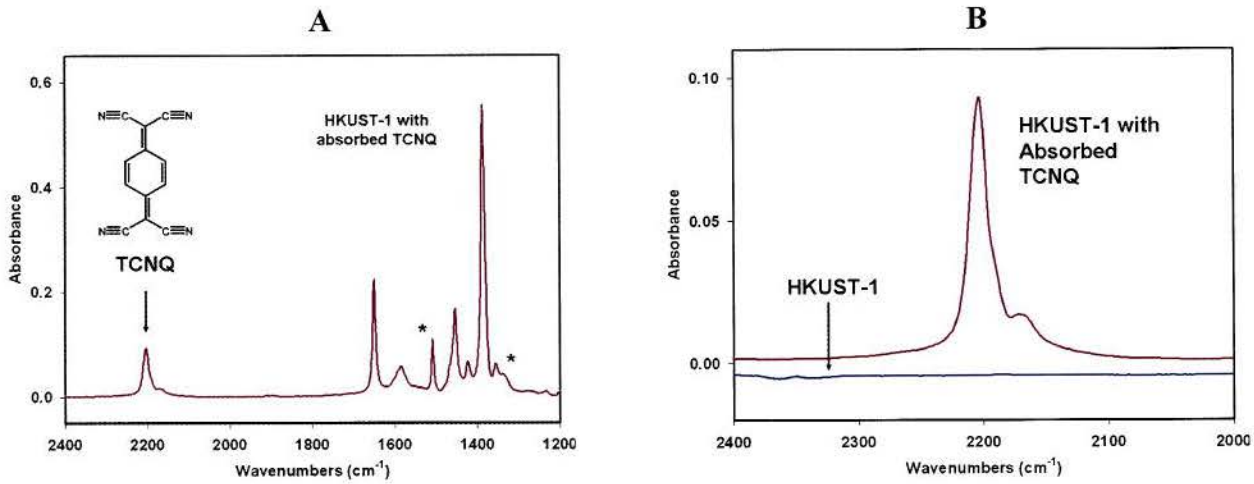

Figure 26. Reflectance FT-IR analysis of a HKUST-1 MOF-SAM on gold after exposure to tetracyanoquinodimethane (TCNQ). **A)** Peaks which arise from the TCNQ molecules are marked in the spectra. **B)** Comparison of HKUST-1 spectra in 2400 to 2000 cm^{-1} region. Blue trace shows HKUST-1 before exposure to TCNQ while the red trace shows the IR spectra after exposure.

Having successfully shown that strongly polar molecules absorb into HKUST-1, we next examined the CWA simulant dimethyl-methylphosphonate (DMMP). This molecule, which is a standard simulant for Sarin and commonly used as an organophosphate with low reactivity and toxicity, was deposited on dehydrated samples of HKUST-1. Exposure was allowed to proceed overnight; on the next day the substrate was rinsed extensively with solvent and dried using nitrogen gas. The thin-film of HKUST-1 was again examined using reflectance FT-IR. The results from these experiments are shown in Figures 27 and 28. All spectra are displayed using the same absorbance scale in order to compare relative peak intensity between the spectra. Figure 27 shows the HKUST-1 film on gold before and after exposure to DMMP. After exposure, intense broad peaks which coincide with oxygen stretching modes of DMMP are found at approximately 1250 cm^{-1} and 1060 cm^{-1}. The mode at 1250 cm^{-1} arises from the ν(P=O) stretching mode while the peaks at 1060 cm^{-1} are due to the methoxy ν(P-O) stretching modes of the molecule. A similar intensity is observed with these peaks when compared to those previously observed with carbon monoxide and TCNQ and may suggest a limiting concentration has been reached. In addition, a small decrease in overall intensity is also observed in several modes arising from the MOF. This effect is observed primarily in the modes appearing at 1381 cm^{-1}, 514 cm^{-1}, and the modes at 758 cm^{-1} and 733 cm^{-1}, however the overall structure of the MOF appears to remain unchanged suggesting DMMP is not reacting with the framework.

After analysis, we attempted to remove the DMMP using a methyl alcohol extraction and vacuum in order to gauge the reversibility of DMMP bonding within the MOF film and whether any permanent changes to the MOF could be observed. The results of this experiment were again examined using FT-IR and are displayed in Figure 28. Shown are IR spectra of the HKUST-1 with the absorbed simulant and after extraction using methanol and vacuum. After extraction, no trace of DMMP is found in the spectrum and the peaks associated with HKUST-1 are found to have returned to their original intensity, suggesting the previously observed changes in the MOF spectra are the result of DMMP bonding in the framework. This result suggests the cause of the previously observed loss of MOF intensity (Figure 27) is due to changes in electron density brought about by the interaction of the electron-rich organophosphate with the copper atoms of the framework. Removal of the DMMP allows the MOF to return to its original state. These results once again confirm that DMMP, due to strongly polar and Lewis acidic phosphorus-oxygen functionality, is able to absorb into the MOF to high concentrations similar to those observed with carbon monoxide and cyano-functionalized TCNQ. In addition, the absorption of DMMP is shown to be fully reversible with the simulant being removed with a simple extraction step followed by exposure to vacuum. These results demonstrate HKUST-1 as a useful nanoporous material capable of absorbing high concentrations of polar molecules selectively over non-coordinating species and could serve as an important new nanomaterial for filtration and sensor applications.

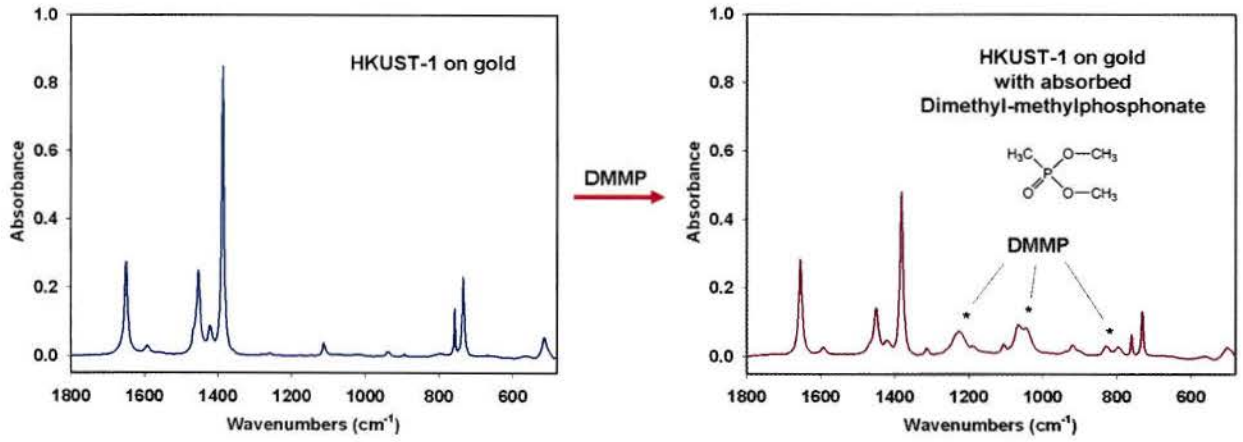

Figure 27. Surface-reflectance FT-IR analysis of a HKUST-1 MOF-SAM on gold before and after exposure to dimethyl-methylphosphonate (DMMP). Peaks which arise from the DMMP molecules are marked in the spectra. High concentrations of DMMP are absorbed by the MOF which shows some loss of absorbance intensity but no permanent changes in structure.

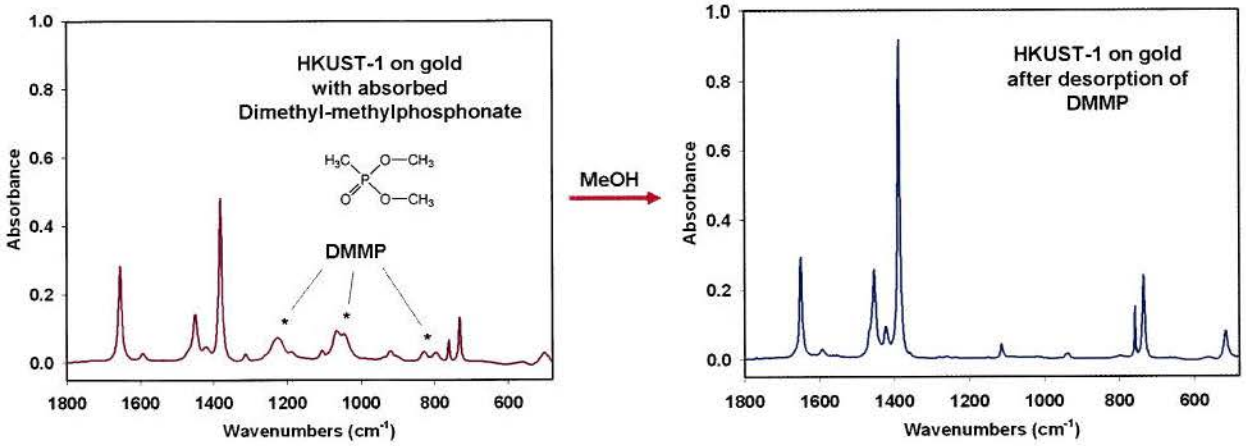

Figure 28. Reflectance FT-IR analysis of HKUST-1 on gold before and after extraction of DMMP. Peaks which arise from the absorbed DMMP are marked in the spectra. After extraction, all traces of the DMMP are removed from the MOF which returns to its original absorbance (see Figure 27). No evidence of permanent changes to the framework structure is observed.

During this time we also began to examine the electronic properties of HKUST-1 thin-films on gold using the microsphere test-bed. The incorporation of MOF films into microsphere junctions could be accomplished by initially functionalizing the magnetic arrays with a monolayer of 4-MBA. The arrays were then sequentially immersed in the 1 mM solutions of copper acetate and trimesic acid until the desired number of layers were deposited, followed by deposition of microspheres in order to close electrical contact across each device and MOF film. After fabrication, the completed devices were placed inside SAIC's semiconductor probe station and placed under vacuum to acquire electron transport data using our Hp Semiconductor parametric analyzer. Figure 29 compares the electron transport properties of HKUST-1 and HKUST-1 with absorbed TCNQ molecules. Typical microsphere junctions incorporating 5 layers of HKUST show electrical resistance around 200-400 MΩ. In the microsphere test bed, this translates to approximately 200-500 pA at 100 mV bias. However, similar devices which incorporate HKUST-1 with absorbed TCNQ molecules displayed much higher conductivity. Multiple HKUST-1 devices which absorbed TCNQ displayed resistance around 40 MΩ. Most devices were found to pass 2-3 nA of current at 100 MV bias or an increase by a factor of 5-10 after absorption of the TCNQ. This result confirms that absorption of organic molecules (in this case an organic semiconductor) can be used to tune the electrical properties of the MOF film under study. We also performed variable temperature I/V measurements on our HKUST-1 films

to test whether they display typical semiconducting behavior. Figure 29b shows the result of these experiments. The plot shows the resistance of a microsphere junction which incorporates a HKUST-1 film with absorbed TCNQ as a function of temperature from 280K to 360 K. The data shows a clear decrease in junction resistance with increasing temperature as is typically found in semiconducting materials (higher temperatures promote electrons into conduction bands within the material). The cause of the non-linear feature centered around 345 K remains unknown but may be related to loss of solvent molecules and annealing processes within of the framework. This data confirms HKUST-1 exhibits electrical properties typical of a wide band-gap semiconductor whose electrical properties can be tuned using absorption of small organic molecules.

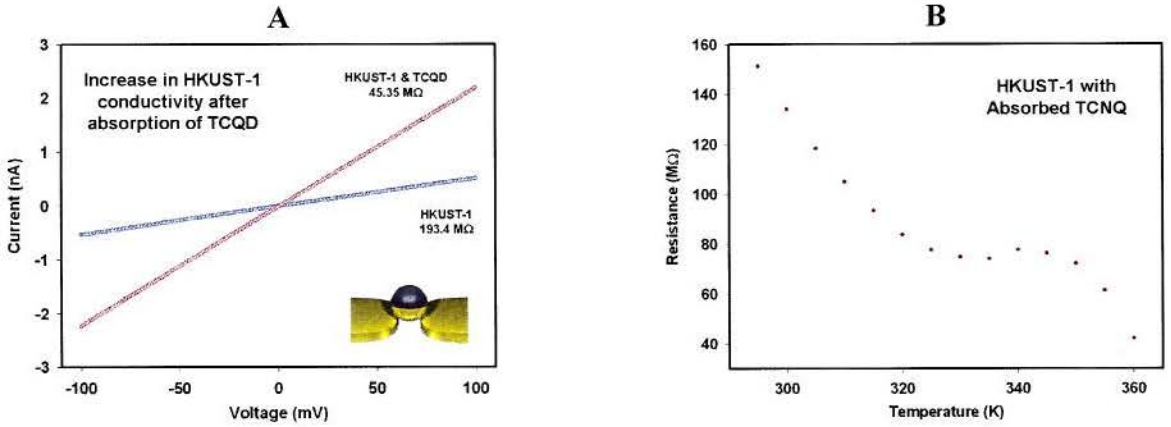

Figure 29. Electron transport properties of HKUST-1 and HKUST-1 with absorbed TCNQ molecules. **A)** Current-voltage I/V properties of HKUST-1 microsphere junctions. An increase in conductivity by a factor of five is attributed to the presence of absorbed TCNQ. **B)** Variable temperature I/V measurements of HKUST-1 with incorporated TCNQ. A decrease in conductivity with increasing temperature is indicative of semiconducting behavior.

An additional experiment examined the electrical properties of dehydrated HKUST-1 molecular junctions under a variety of gaseous atmospheres. The results of which are shown in Figure 30. Molecular junctions incorporating HKUST-1 were extensively dehydrated under high vacuum conditions (1×10^{-6} torr) for two days. After dehydration, the devices were examined under vacuum to acquire baseline transport properties. After measuring the current-voltage properties under vacuum, the chamber was backfilled with various gases and the devices reexamined in order to determine the influence the absorption of each gas had on the conductivity of the HKUST-1 thin film. After exposure to each gas and measurement of I/V

data, the chamber was again evacuated to high-vacuum in order to remove all absorbed gas and prepare the nanoscale devices for the next gas. Our experiments typically examined inert or non-reactive gases first, followed by those which would be expected to show increased interaction with the MOF. Figure 30 displays several of the gases tested. As expected, argon and nitrogen atmospheres showed little interaction with the MOF. I/V data acquired under inert gases displayed resistances similar to those measured under high vacuum conditions. Gases with increasing interaction with the open copper sites in the material, however, influenced the materials conductivity the greatest as seen by the change in MOF I/V properties under carbon monoxide, as gas known to absorb readily into HKUST-1 (Figure 25). Given the selectivity of HKUST-1 and other MOF materials for polar molecules, it would be expected that these material will display a large change in resistance after exposure to CW agents and simulants such as DMMP. The strong Lewis acidity of these molecules will bind strongly to the interior of the MOF, causing large changes in electron density at the metal center and the coordination bonds which serve as the orbital pathways for electrons. Since the binding of polar molecules in MOF materials will naturally influence the very bonds which carry charge under an applied bias, the development of metal-organic frameworks into a new class of sensing material is theoretically possible. The results shown here have demonstrated proof-of-principle for this application as well as possible applications for MOF materials in filtration or selective molecule absorption for air-purification systems.

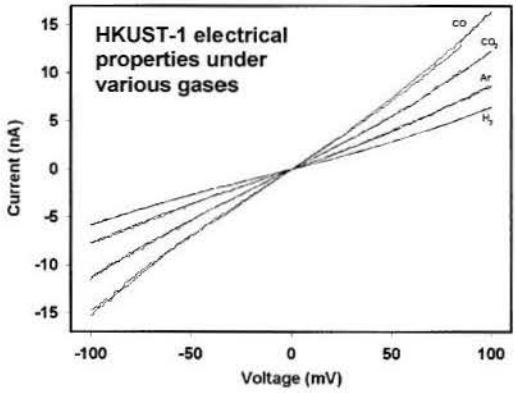

Figure 30. Current-voltage properties of HKUST-1 under various atmospheric conditions. The nature of the molecular species inside the nanoporous MOF influences the conductivity of the material and could be the basis for a new sensor system.

Our research ending in July 2009 focused primarily on use of the metal-organic framework $Cu_3(BTB)_2$. This MOF displays larger internal pore size compared to HKUST-1, with overall internal dimensions of 7.6 × 14 Å (Figure 31) which should allow the absorption of larger organic molecules and CWA simulants into the MOF structure. Deposition of $Cu_3(BTB)_2$ proceeded as previously described for HKUST-1. Reflectance FT-IR analysis was then used to confirm the growth of the MOF on the surface. Figure 32 illustrates our results obtained on a thin-film of $Cu_3(BTB)_2$ incorporating 30 layers. As found previously with HKUST-1, the primary peaks observed in the IR of this material arises from the Cu-carboxyl linkages formed during self-assembly of the MOF on the surface. In order to test whether this material could indeed absorb large organic molecules, we exposed a dehydrated thin-film of $Cu_3(BTB)_2$ to the VX simulant Demeton-S ($C_6H_{15}O_3PS_2$). 30 layers of $Cu_3(BTB)_2$ deposited on gold were exposed to vapor from Demeton-S inside a sealed vial for a period of 24 hrs. After this time the substrate was removed and transferred to an inert-atmosphere FT-IR spectrometer for analysis. Figure 32b shows the results of our spectroscopic experiment.

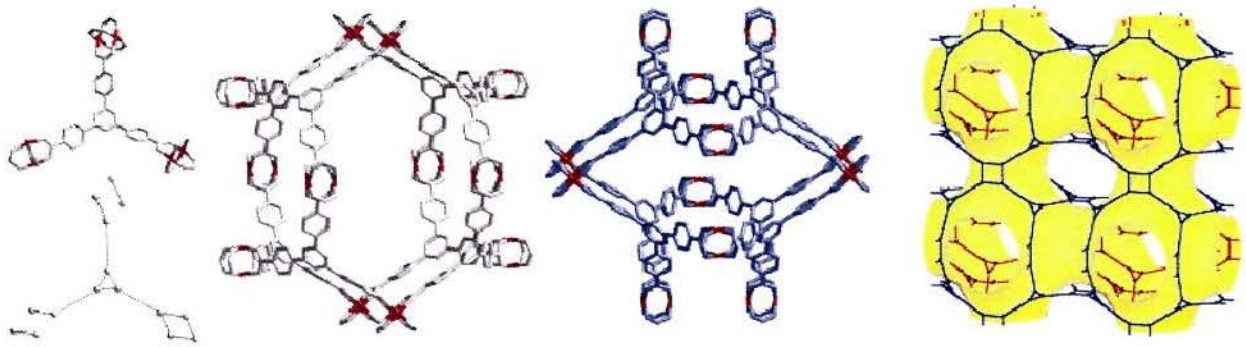

Figure 31. Illustrations showing the structure of the metal-organic framework $Cu_3(BTB)_2$ which incorporates nanoscale cavities 7.6 × 14 Å. Illustrations adapted from Chen B. *Science*, 2001, 291, 1021.[22]

Figure 32a shows the $Cu_3(BTB)_2$ MOF film before exposure to Demeton-S while Figure 32b shows the same film after exposure to the simulant vapor for 24 hrs. After exposure, intense peaks which coincide with oxygen stretching modes of Demeton-S are found at approximately 1260 cm^{-1} and 1040 cm^{-1}. The mode at 1260 cm^{-1} arises from the ν(P=O) stretching mode while the peaks at 1040 cm^{-1} are due to the methoxy ν(P-O) stretching modes of the molecule. In

addition, a small decrease in overall intensity is also observed in several modes arising from the MOF which was also observed in the HKUST-1 after absorption of the simulant DMMP and may be the result of changing electron density as the MOF absorbs the strong Lewis Basic organophosphate.

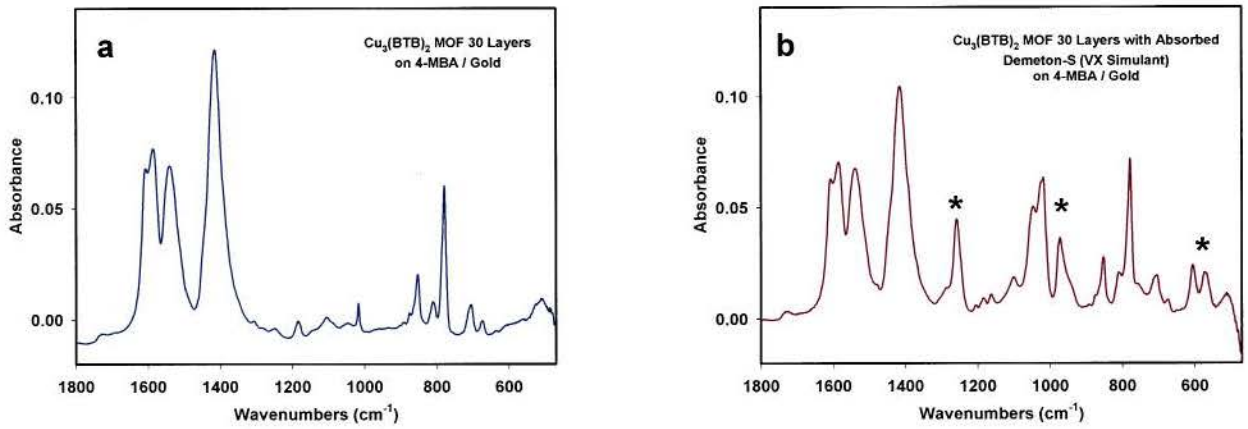

Figure 32. Surface-reflectance FT-IR analysis of $Cu_3(BTB)_2$ on gold before and after exposure to Demeton-S, a simulant for VX. Peaks which arise from the simulant molecules are marked in the spectra. High concentrations of simulant are absorbed by the MOF which shows some loss of absorbance intensity but no permanent changes in structure.

Conclusion:

This research examined the interaction of gaseous chemical agents with self-assembled monolayers held within molecular junctions and measured the vibrational and electronic effects induced in the nanoscale metal-molecule-metal devices. Changes in electron transport through incorporated SAMs were correlated to chemical interactions observed in the organic monolayers using reflectance FT-IR on functionalized gold substrates. Real-time current-voltage measurements, coupled with reflectance FT-IR have been combined to yield valuable information as to the effects of interactions occurring between functionalized self-assembled monolayers immobilized in molecular junctions and gaseous chemical agents present in the environment. This information could yield valuable information for the possible development of nanoscale sensors based on molecular conductance and organic receptors.

References:

1. J. M. Tour, *Molecular Electronics: Commercial Insights, Chemistry, Devices, Architectures and Programming* (World Scientific, River Edge, New Jersey, 2003).
2. R. L. Carroll, C. B. Gorman, *Angew. Chem. Int. Edn.* 2002, *41,* 4378.
3. Y. Selzer, *et al. Nano Lett.* 2005, *5,* 61.
4. Y. Selzer, A. Salomom, D. Cahen, *J. Phys. Chem. B* 2002, *106,* 10432.
5. H. Basch, R. Cohen, M. Ratner, *Nano Lett.* 2005, *5,* 1668.
6. V. Chechik, R. Crooks, C. Stirling, *Adv. Mater.* 2000, *12,* 1161.
7. A. Ulman, *Chem. Rev.* 1996, *96*, 1533.
8. D. Karpovich, G. Blanchard, *Langmuir* 1997, *13*, 4031.
9. U. H. Pi, *et al. Surf. Sci.* 2005, *583*, 88.
10. D. Long, *et al. Appl. Phys. Lett.* 2005, *86*, 153105.
11. J. Kushmerick, A. Blum, D. Long, *Anal. Chim. Acta.* 2006, *568*, 20.
12. B. Boer *et al. Langmuir* 2004, *20*, 1539.
13. G. Fisher *et al. J. Amer. Chem. Soc.* 2002, *124*, 5528.
14. J. Choi, Y. Zhao, D. Zhang, S. Chien, Y. H. Lo, *Nano Letters* 2003, *3*, 995.
15. J. C. Love, B. Gates, D. Wolfe, K. Paul, G. Whitesides, *Nano Letters* 2002, *2*, 891.
16. J. C. Love, L. Estroff, J. Kriebel, R. Nuzzo, G. Whitesides, Chem. Rev. 2005, *105*, 1103.
17. J. Tour *et al. Chem. Eur. J.* 2001, *7*, 5118.
18. J. Tour, *Chem. Rev.* 1996, *96*, 537.
19. A. S. Blum, *et al. Nature Materials* 2004, *4*, 167.
20. D. Long *et al. Nature Materials* 2006, 5, 901-908.
21. Shekhah, O. *et al. J. Amer. Chem. Soc.* 2007, *129*, 15118.
22. Chen B. *et al. Science*, 2001, 291, 1021.